AD-A072 690 NAVAL POSTGRADUATE SCHOOL MONTEREY CA F/G 11/4
COMPRESSIVE FATIGUE IN GLASS AND GRAPHITE REINFORCED COMPOSITES--ETC(U)
JUN 78 J D CONNERS

UNCLASSIFIED NL

1 OF 2
AD
A072690

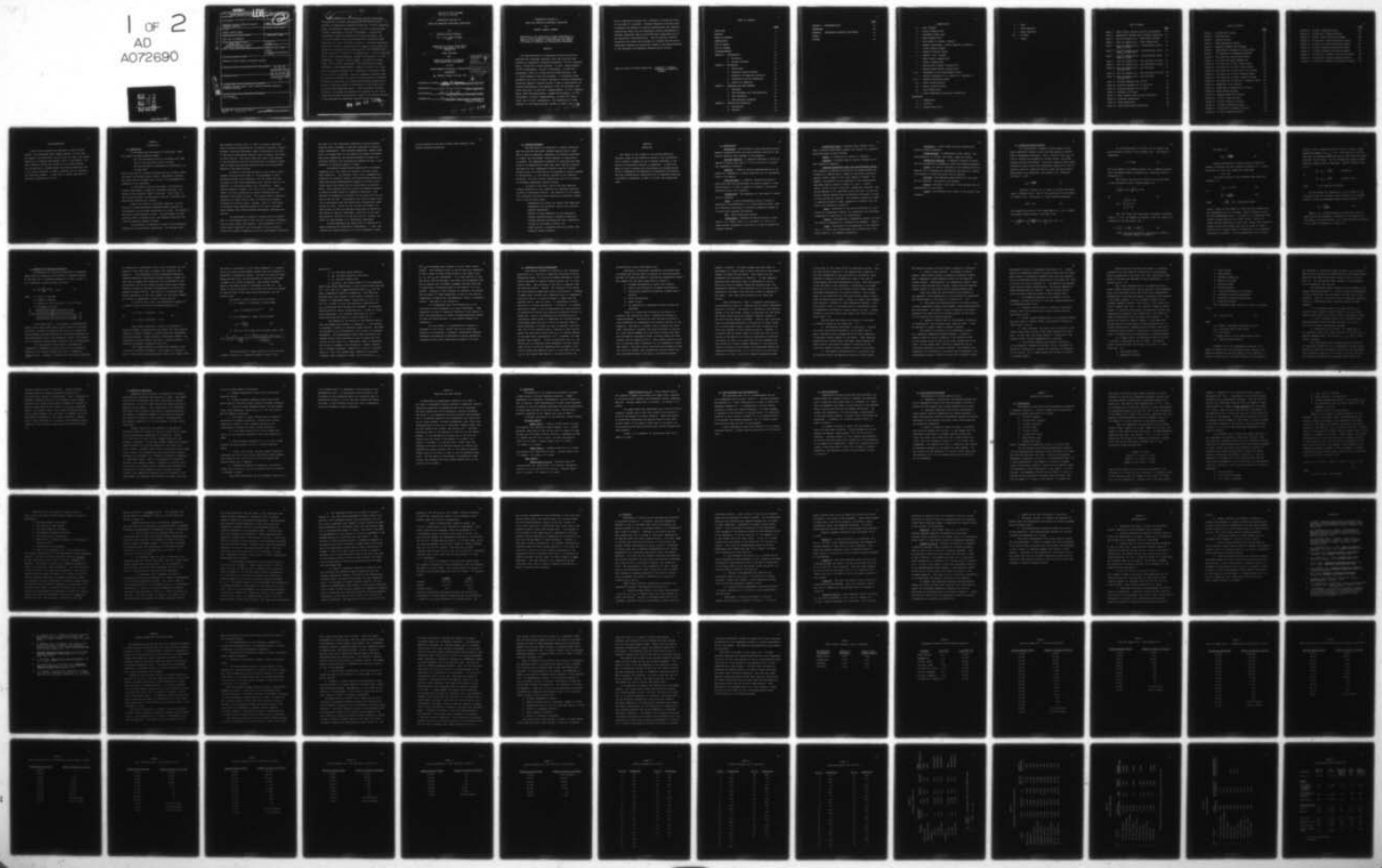

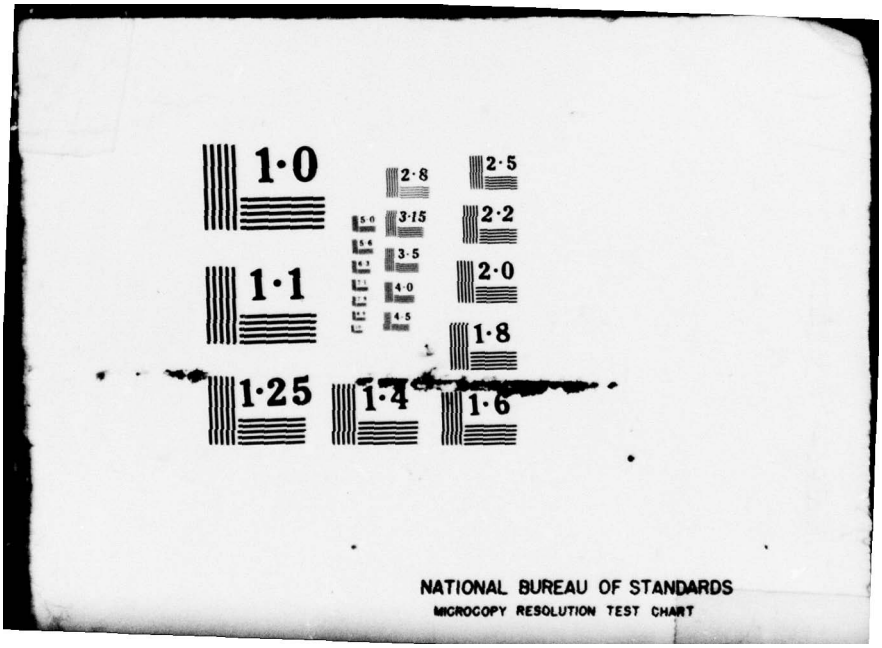
1·0
1·1
1·25
2·8
3·15
3·5
4·0
4·5
2·5
2·2
2·0
1·8
1·4
1·6
NATIONAL BUREAU OF STANDARDS
MICROCOPY RESOLUTION TEST CHART

UNCLASSIFIED

SECURITY CLASSIFICATION OF THIS PAGE (When Data Entered)

LEVEL

REPORT DOCUMENTATION PAGE

READ INSTRUCTIONS BEFORE COMPLETING FORM

1. REPORT NUMBER	2. GOVT ACCESSION NO. / 3. RECIPIENT'S CATALOG NUMBER
4. TITLE (and Subtitle) COMPRESSIVE FATIGUE IN GLASS AND GRAPHITE REINFORCED COMPOSITES	5. TYPE OF REPORT & PERIOD COVERED THESIS 6. PERFORMING ORG. REPORT NUMBER
7. AUTHOR(s) CONNERS, JEFFREY DURNELL	8. CONTRACT OR GRANT NUMBER(s)
9. PERFORMING ORGANIZATION NAME AND ADDRESS MASS. INST. OF TECHNOLOGY	10. PROGRAM ELEMENT, PROJECT, TASK AREA & WORK UNIT NUMBERS
11. CONTROLLING OFFICE NAME AND ADDRESS Code 031 NAVAL POSTGRADUATE SCHOOL MONTEREY, CALIFORNIA, 93940	12. REPORT DATE JUN 78 13. NUMBER OF PAGES 120
14. MONITORING AGENCY NAME & ADDRESS(if different from Controlling Office)	15. SECURITY CLASS. (of this report) UNCLASS 15a. DECLASSIFICATION/DOWNGRADING SCHEDULE

16. DISTRIBUTION STATEMENT (of this Report)

APPROVED FOR PUBLIC RELEASE; DISTRIBUTION UNLIMITED

17. DISTRIBUTION STATEMENT (of the abstract entered in Block 20, if different from Report)

DDC RECEIVED AUG 14 1979 D

18. SUPPLEMENTARY NOTES

19. KEY WORDS (Continue on reverse side if necessary and identify by block number)

COMPRESSIVE FATIGUE, FATIGUE, GLASS & GRAPHITE REINFORCED COMPOSITES, REINFORCED COMPOSITES

20. ABSTRACT (Continue on reverse side if necessary and identify by block number)

SEE REVERSE

AD A072690

DDC FILE COPY

DD FORM 1 JAN 73 1473 EDITION OF 1 NOV 65 IS OBSOLETE
S/N 0102-014-6601 |
(Page 1)

UNCLASS
SECURITY CLASSIFICATION OF THIS PAGE (When Data Entered)

The characteristics of compressive fatigue failure are described for unnotched laminates, with the following rank ordering by compressive strengths determined: [0°/90°] Graphite/Epoxy, [0°/±45°/90°] Graphite/Epoxy, [0°/±45°] Graphite/Epoxy, [0°/90°] Glass/Epoxy, [0°/±45°] Glass/Epoxy, [0°/±45°/90°] Glass/Epoxy, Style 61 E Glass Woven Rovings/Polyester, and 1.5 ounce Chopped E Glass Mat/Polyester. A normalized slope parameter with units of percent decrease of ultimate compressive stress per decade of applied cycles is used to characterize the fatigue resistances of the materials, with the following rank order resulting: [0°/±45°/90°] Graphite/Epoxy, [0°/90°] Graphite/Epoxy, Woven Roving/Polyester, Chopped Mat/Polyester, [0°/90°] Glass/Epoxy, [0°/±45°] Graphite/Epoxy, [0°/±45°/90°] Glass/Epoxy, and [0°/±45°] Glass/Epoxy. The degradation by water immersion of the Graphite/Epoxy systems is shown to be a loss static compressive strength and a decrease in normalized slope on the order of 10 percent. Multiple Regression Analysis used to quantify the effects of varying unidirectional ply laminate orientations shows that the compressive fatigue resistances of advanced composites cannot be satisfactorily explained only by ply orientation characterization. Various physical theories concerning the causes and processes of ultimate failure during compressive fatigue are postulated, based on the microstructures of the specimens and phenomena observed during testing.

(6)

COMPRESSIVE FATIGUE IN GLASS AND GRAPHITE REINFORCED COMPOSITES

by

(10) Jeffrey Durnell/Conners

B.S., U.S. Naval Academy
(1971)

(9) Masters thesis,

Submitted in partial fulfillment
of the requirements for the
degrees of

(12) 122 p.

Ocean Engineer

and

Master of Science in Shipping
and Shipbuilding Management

at the

Massachusetts Institute of Technology

(11) June, 1978

Accession For	
NTIS GRA&I	X
DDC TAB	☐
Unannounced	☐
Justification	
By	
Distribution/	
Availability Codes	
Dist	Avail and/or special
A	

Signature of Author Jeffrey D. Conners
Department of Ocean Engineering, May 1978

Certified by _____
Thesis Supervisor

Certified by Kenneth Thomas
Ocean Engineering Department Reader

Accepted by _____
Chairman, Departmental Committee on
Graduate Students

COMPRESSIVE FATIGUE IN GLASS AND GRAPHITE REINFORCED COMPOSITES

by

JEFFREY DURNELL CONNERS

Submitted to the Department of Ocean Engineering on May 12, 1978 in partial fulfillment of the requirements for the Degrees of Ocean Engineer and Master of Science in Shipping and Shipbuilding Management.

ABSTRACT

The characteristics of compressive fatigue failure are described for unnotched laminates, with the following rank ordering by compressive strengths determined: [0°/90°] Graphite/Epoxy, [0°/±45°/90°] Graphite/Epoxy, [0°/±45°] Graphite/Epoxy, [0°/90°] Glass/Epoxy, [0°/±45°] Glass/Epoxy, [0°/±45°/90°] Glass/Epoxy, Style 61 E Glass Woven Rovings/Polyester, and 1.5 ounce Chopped E Glass Mat/Polyester. A normalized slope parameter with units of percent decrease of ultimate compressive stress per decade of applied cycles is used to characterize the fatigue resistances of the materials, with the following rank order resulting: [0°/±45°/90°] Graphite/Epoxy, [0°/90°] Graphite/Epoxy, Woven Roving/Polyester, Chopped Mat/Polyester, [0°/90°] Glass/Epoxy, [0°/±45°] Graphite/Epoxy, [0°/±45°/90°] Glass/Epoxy, and [0°/±45°] Glass/Epoxy. The degradation by water immersion of the Graphite/Epoxy systems is shown to be a loss

static compressive strength and a decrease in normalized slope on the order of 10 percent. Multiple Regression Analysis used to quantify the effects of varying unidirectional ply laminate orientations shows that the compressive fatigue resistances of advanced composites cannot be satisfactorily explained only by ply orientation characterization. Various physical theories concerning the causes and processes of ultimate failure during compressive fatigue are postulated, based on the microstructures of the specimens and phenomena observed during testing.

Name and Title of Thesis Supervisor: Frederick J. McGarry,
Professor of Materials
Science

TABLE OF CONTENTS

Nomenclature

A - area (inches^2)

E - Young's modulus (psi)

F - allowable stress (psi)

G - shear modulus (psi)

I - area moment of inertia (inches^4)

K - general coefficient, usually denoting a constant

L - column length (inches)

N - number of fatigue cycles

P - applied load (pounds)

γ - shear strain (inches/inch)

ε - strain (inches/inch)

σ - applied axial stress (pounds/inch^2)

τ - applied shear stress (pounds/inch^2)

u,v,w - components of the displacement vector

θ - angular orientation of a lamina in a laminate (°)

x,y,z - general coordinate system

k_f - fiber volume fraction

k_m - matrix volume fraction

k_v - void volume ratio

β - theory-experiment correlation coefficient

SUBSCRIPTS:

c - compression

cr - critical

$p\ell$ - proportional limit

s - shear

f - fiber material

m - matrix material

ult - ultimate

ℓ - lamina

LIST OF TABLES

LIST OF FIGURES

Acknowledgements

I would like to express my gratitude to the following people: to my beautiful wife, Debbie Conners, for her love, her support, her motivation, and last but not least, her typing services; to Professor Fred McGarry and Dr. John Mandell, for their technical advice and counsel; to Mr. Arthur Rudolph, for his services in manufacturing the gripping mechanism; and to Mr. Harold Edelstein of NSRDC, Annapolis for his technical and logistical support. I hope that my effort here does not seriously disappoint any of you.

CHAPTER 1

Introduction

A. Motivation

In the design and fabrication of structures, there are always two basic questions asked:

- will the structure be able to withstand the loads that it will encounter without failing?
- can the structure be designed more efficiently, or at less cost?

Even in the case of a simple structure such as a bridge, there are static and dynamic loads, tensile, compressive, bending, and shear loads to contend with, as well as environmental degradation of the structure.

In the design of marine structures, the process is further complicated: because of Archimedes principle, the weight of the structure itself is critical. Very simply, in any floating vehicle, the less weight used for structure, the more weight available for payload.

Before the advent of "advanced" materials, the designer of a marine structure addressed himself primarily to the selection of the proper scantlings to be used. The material was nearly always limited to steel. The development of high strength steels, aluminum alloys, and composite materials has given the designer greater latitude.

The selection of materials is based on the properties required for the particular application. As has been noted,

the strength-to-weight ratio is often of primary importance. Other controlling properties may be fracture toughness, fatigue strength, corrosion resistance, ease of fabrication, and cost. In the case of homogeneous materials such as metals, the choice is often obvious: most ships today have steel hulls because of the availability and all-around good mix of physical properties of steels and aluminum superstructures are incorporated because of the weight savings.

In the past few years advances in the field of hydrodynamics have paralleled those in the development of high strength-to-weight ratio materials, and the result has been the advent of the "high performance naval vehicle" such as the hydrofoil or the Surface Effect Ship (hovercraft). These vehicles depend on dynamic lift (foils or air cushions, respectively) for their propulsion and speed advantages and are therefore very weight critical. The current trend in materials selection for these vehicle types is towards high strength aluminum and titanium alloys. However, there is a new family of materials being developed primarily for use in the aerospace industry that offers promising advantages: advanced composites.

The advantages of composites accrue from the development of high-strength and/or high modulus, continuous filaments, such as glass, boron, and graphite; the development of improved matrix materials; and the concept of using uniaxial, stabilized columnar filamentary arrays as load-bearing structures.

The idea is to use cross-plied laminates to tailor material strength and/or stiffness to specific envelopes of stress or strain requirements. With advanced composites a design flexibility is created that is not possible with metal structures. When using composites, the designer becomes not merely the materials selector, but the materials designer as well; a new dimension in structural design is added.

One specific current marine application of advanced composites is in the strut-foil system of the PCH (Patrol Craft Hydrofoil). The hydrofoil with a fully submerged foil system and an automatic control and stabilization system provides boat motion characteristics superior to those of much larger ships, even those with fin stabilizers or anti-roll tanks. This platform stability allows the ordnance system to be effective under nearly all operating conditions. The selection of materials is critical for the strut and foil, as well as for the hull. The material must survive impact loading in negotiating high sea states while foilborne and crash landing in waves. HY-80, HY-100, HY-130, and Inconel 718 steel alloys, as well as aluminum alloys such as 5456-H-116 and 5456-H-117 have all been used. Since 50% of the light ship weight of the PCH is in the hull and foil systems, the weight of these systems is of significant importance.

Studies addressing the application of composites to these structures are contained in References 1, 2, and 3 and indicate that weight savings of up to 60% compared to steel

can be realized by the use of hybrid high-strength, high-modulus graphite composites.

B. Problem Statement

The application of composites to complex structures such as hulls and strut-foil systems requires that a large body of data be generated, addressing all possible conditions of loading and environment (water immersion in particular). In general, the compressive strengths of composites have been found to be substantially lower than their tensile strengths, and hence not only compressive fatigue lives but flexural fatigue lives are controlled by the compressive fatigue strength of the material. In the working lifetime of any composite structure, its most critical property may well be its ability to withstand compressive fatigue loading.

In spite of this fact, one of the most neglected loading conditions in the literature for composite materials is that of compressive fatigue. The objective of this thesis is to partially alleviate that condition by providing information in the following areas:

- Compressive S-N curves for typical GRP composites,
- Compressive S-N curves for typical high strength graphite composites,
- Effects of water immersion on the compressive fatigue characteristics of graphite composites,
- Optimum laminate configurations where compressive fatigue is the primary loading, and
- Other factors or parameters which may affect compressive fatigue strength.

CHAPTER 2

Background

The intent of this chapter is to further define the technical scope of the problem as stated in the introduction and to present a summary of the literature pertinent to the subject of compressive fatigue in composites. A definitive basis on which to pursue the investigation is thereby gained. Prior to addressing the mechanics of compression and buckling and the micromechanical characteristics of composite materials, a glossary is presented in order to clarify the terminology used.

A. Definitions

Anisotropic - Not isotropic; having mechanical and/or physical properties which vary with direction relative to the natural reference axes inherent in the material.

Balanced Laminate - A composite laminate in which all laminae at angles other than 0° or 90° occur only in ± pairs (not necessarily adjacent).

Buckling - A mode of failure characterized by an unstable and unsymmetrical lateral deflection due to compressive force on the sample.

Coupling Agent - A chemical substance designed to react with both the reinforcement and matrix phases of a composite material to form or promote a stronger or more water resistant bond at the interface.

Delamination - The separation of the layers of materials in a laminate.

Fiber - A single homogeneous strand of material, essentially one-dimensional in the macro-behavior sense, used as a principle constituent in advanced composites because of its high axial strength and modulus.

GRP - Glass Reinforced Plastics.

Interlaminar - Descriptive term pertaining to some object (i.e. voids), event (i.e. fracture), or field (i.e. shear stress) referenced as existing or occurring between two adjacent laminae.

Interlaminar Shear - Shearing force tending to produce a relative displacement between two laminae in a laminate along the plane of their surface.

Lamina - A single ply or layer in a laminate.

Laminate - A product made by bonding together two or more laminae of material.

Laminate Orientation Code (for unidirectional plies) - Each laminate is defined by indicating the proportionate distribution of laminae among a number of specified orientation angles, without regard to the total number of laminae. For example, the specific lay-up sequences of the unidirectional laminates used are shown in Tables 2,3, and 4. Figure 1 shows a sketch of the [0°/±45°/90°] symmetrical laminate. The lay-up sequence is not specified using this code, so that the actual stacking sequence must be specified ply-by-ply in order to fully define the laminate. The cross-ply angles are listed in ascending numerical order, separated by slashes, with the entire list enclosed by brackets.

Macro - Pertaining to the gross properties of a composite as a structural element, not considering the individual properties or identities of the constituents.

Matrix - The essentially homogeneous material in which the fibers or filaments of a composite are embedded. (Resin)

Micro - Pertaining to the properties of the constituents, i.e. matrix and reinforcement and interface only, and their effect on the composite properties.

Orthotropic - Having three mutually perpendicular planes of elastic symmetry.

Preimpregnated - A combination of mat, fabric, non-woven material, or roving, with resin, ready for curing.

Symmetrical Laminate - A composite laminate in which the ply orientation is symmetrical about the laminate midplane.

X-axis - An axis in the plane of the laminate which is used as the 0° reference for designating the angle of a lamina. The direction in which the axial load is applied.

XY Plane - The reference plane parallel to the plane for the laminate. The plane of the laminae.

Y-axis - The axis in the plane of the laminate that is perpendicular to the X-axis.

Z-axis - The reference axis normal to the plane of the laminate.

B. Classical Buckling Theory

On a macro-scale, composite columns appear to fail under compressive loading in much the same manner as columns made of homogeneous materials: when a critical value (P_{cr}) of load is reached and exceeded by a slight amount, the column becomes unstable and buckles. Using the classical Euler column formulation which solves the differential equation for the deflection curve of a beam with built-in ends (as most closely approximates this experiment; see Chapter 3-B), Timoshenko and Gere (4) give:

$$P_{cr} = \frac{4\pi^2 EI}{\ell^2} \qquad [1]$$

Rayleigh's method, for a column of uniform stiffness, takes a different tack - that of the application of the method of virtual work. Den Hartog (5), using the Euler equation

$$EIy'' = -Py \qquad [2]$$

and assuming the slope of the loaded beam is $y = f(x)$, showed the bending energy stored in the beam to be:

$$U = \int_0^{\ell} \frac{M^2}{2EI}\,dx = \int_0^{\ell} \frac{(EIy'')^2}{2EI}\,dx = \frac{1}{2}\int_0^{\ell} EI(y'')^2 dx \qquad [3]$$

If the cross-section is uniform, EI is constant and can be brought in front of the integral sign. The energy of compression

$$U = P^2 \ell / 2AE \qquad [4]$$

has to be added to the bending energy, but it remains constant while the bending energy increases with increasing buckling deflection (y).

The virtual work done by P then has to be equivalent to the incremental elastic bending energy, so:

$$P \frac{1}{2} \int_0^{\ell} (y')^2 dx = \frac{1}{2} \int_0^{\ell} EI(y")^2 dx$$

or, [5]

$$P_{cr} = \frac{\int_0^{\ell} EI(y")^2 dx}{\int_0^{\ell} (y')^2 dx}$$

Now, for a beam with fixed ends, we assume a deflected shape (y = f(x)) as general as possible, such that there is no curvature at the end points, say:

$$y = y_o \left[1 + A \frac{x}{\ell/2}^2 + B \frac{x}{\ell/2}^4 \right] \qquad [6]$$

(Note: with this derivation, the origin is taken at mid-span because of symmetry)

The result is:

$$P_{cr} = \frac{168EI}{17\ell^2} \qquad [7]$$

Another methodology is that of using an effective length of the beam (ℓe) and a radius of gyration (r). Pilkey and Pilkey (6) give, for a beam with fixed ends

$$\ell e = .65\ell$$

The Euler solution to the fixed-end beam under compression, is

$$P_{cr} = 2.37\pi^2 EI \qquad [7a]$$

or,

$$\frac{P}{A} = \frac{\pi^2 E}{(\ell e/r)^2} \qquad [7b]$$

where $I = \frac{bh^3}{12}$ (for a rectangular beam)

Figure 7 shows how the method of column buckling depends upon the slenderness ratio of the beam. Euler's formula is valid for high slenderness ratios. In Figure 7 it is seen that very slender columns buckle at low stress levels. The use of higher strength materials will not fully correct this condition, however the critical stress level can be raised by using a material with a higher modulus of elasticity or by increasing the radius of gyration. For low slenderness ratios, column

failure is due to material failure; the bar becomes a simple compression member, and $\sigma_{ult} = P/A$. From Table 16 it can be seen that the specimen geometries used in this study all nearly represent "short" beams. For the intermediate length columns empirical formulas must be developed. Typical formulas would be (6)

$$\frac{P}{A} = \sigma_{ult} - D\left(\frac{\ell e}{r}\right)^2 \qquad \text{(parabolic)}$$

or

$$\frac{P}{A} = \sigma_{ult} - D\left(\frac{\ell e}{r}\right) \qquad \text{(straight line)}$$

where D is an empirical constant.

One last method for determining σ_{cr} for columns in the inelastic range is to replace Young's modulus E by a tangent modulus, giving the Engresser tangent modulus formula (4):

$$\sigma_{cr} = \frac{\pi^2 E_r}{(\ell e/r)^2} \qquad [7c]$$

Where E_r is a "reduced modulus of elasticity" that depends both on the mechanical properties of the material and the shape of the cross-section. For a more detailed explanation of E_r, refer to reference (4), page 176.

C. Mechanics of Composite Materials

An adaptation of the Euler formulation to composite beams simply by explaining the stiffness or bending rigidity of the beam (EI) in "laminate language" is given in Dietz (7). For a composite isotropic column, he gives

$$EI = \frac{2}{3} b \sum_{m=1}^{n} E^m (h_m^3 - h_{m-1}^3) \qquad [8]$$

where b = width of the beam

2n = number of laminae

E = modulus in the x direction of the m^{th} layer

h = thickness of plate

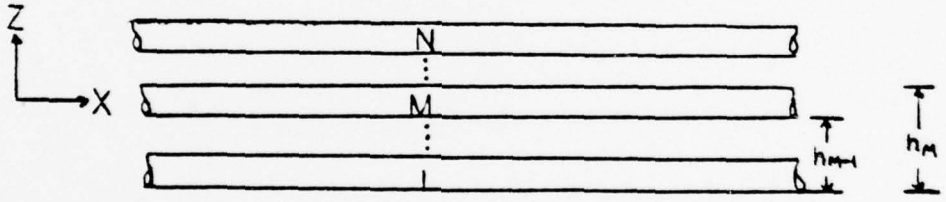

Dietz admits that "...the algebraic transformations become quite lengthy when there are many layers of different materials", however his approach does serve as a theoretical bridge between the macro-analysis of the Rayleigh approach and the micro-analysis used in the theoretical study of the mechanics of composites (herein after referred to as "micromechanics").

For the purpose of this section, the mechanical phenomenon of compressive fatigue failure will be viewed as essentially and closely related with that of compressive static failure. Broutman (8) states that the fatigue strengths

of composites are governed by their static strengths, and the results of this study tend to support that assertion (see Chapter 4). The predominant failure mechanisms observed in composite materials experiencing fatigue loading (Chapter 2-D) also tend to support the contention that the mechanical precipitousness with which ultimate failure occurs under fatigue loading is caused by the same micromechanisms as static compressive ultimate failure. The failure of composites under static compression is also very sudden, and the failed samples are similar in appearance to failed fatigue samples.

At the most basic level, the compressive strength of a lamina is given by the Rule of Mixtures equation (4):

$$\sigma_\ell = \sigma_f(k_f + k_m(E_m/E_f)); \quad \varepsilon_f<\varepsilon_m$$

or [9]

$$\sigma_\ell = \sigma_m(k_m + k_f(E_f/E_m)); \quad \varepsilon_f>\varepsilon_m$$

This simple formulation, called the "Strength of Materials Method" illustrates how the matrix and fiber material operate in concert, however it ignores three very fundamental failure mechanisms: fiber buckling, interlaminar effects, and fiber-matrix bonding effects (the bond is assumed perfect). It therefore represents a degenerate case only.

This simple analysis is refined and expanded in the so-called "Microbuckling Method". Both Jones (9) and Broutman (8) offer similar analyses based on the work of Rosen (1965).

The model is postulated as stiff fibers embedded in a comparatively soft matrix which become unstable when the composite is subjected to compressive loading. The load at which the fibers become unstable (P_{cr}) can be estimated by treating the fibers as beams in an elastic foundation. The analysis proceeds based on the energy method of Timoshenko and Gere (4). The change in strain energies for the fibers and matrix are equated to the work done by the fiber during deformation into the buckled state.

The results of this analysis are as follows:

a) For symmetric (transverse) failure modes:

$$\sigma_{ult} = 2k_f(k_f E_m E_f / 3(1-k_f))^{1/2} \qquad [10]$$

b) For nonsymmetric (shear) failure modes:

$$\sigma_{ult} = \frac{G_m}{(1-k_f)} \qquad [11]$$

c) With the void volume ratio included (Foye, 1966):

$$\sigma_{ult} = \left[\frac{G_m}{(1-k_f) + k_f\left(\frac{G_m}{G_f}\right)}\right] \times \left[\frac{1 - \left[2(k_v/(1-k_f))\right] + (k_v/(1-k_f))^2}{1 + \left[\frac{k_v}{(1-k_v)}\right]}\right] \qquad [12]$$

The significance of these equations is that the compressive strength of a composite generally ought to be a

function of:

1) k_f, the fiber volume fraction

2) G_m, the shear modulus of the matrix

3) k_v, the void volume ratio

4) E_m and E_f, the Young's Modulii of the components

Beyond these gross observations it must be noted that equations [10], [11], and [12] do not accurately predict σ_{ult} for the static compressive loading of composites. Both Jones and Broutman carry the analysis a step further, including "influence" or "experiment-theory" coefficients in [10], [11], and [12] in order to force the theoretical predictions of σ_{ult} to correlate with the empirical evidence. For example, the microbuckling theory "correlates well" to data for boron-epoxy composites if an influence coefficient of .63 is multiplied times the modulii in these equations (9).

The reasons for the failure of this analysis derive from the assumptions necessary to complete it. The laminate is presumed to consist of perfectly bonded laminae. The bonds are presumed to be infinitesimally thin as well as non-shear-deformable. The displacements across lamina boundaries are thereby forced to be continuous so that no lamina can slip relative to the other (i.e. interlaminar shear is neglected). Each lamina is assumed to be orthotropic, linearly elastic, and of constant thickness. Referring to Figure 5, displacements u,v, and w are assumed small compared to the plate thickness (small deflection theory) and the strains ε_x, ε_y,

and γ_{xy} are assumed small compared to unity (small strain theory). Only stresses acting in the XY plane are considered so that a state of plane stress exists in the lamina (only σ_x, σ_y, and τ_{xy} are considered). It is also implicit in the derivation that the specimen, the grips, and the applied load are all perfect and in perfect alignment and that there are no impurities or discontinuities in the material or on its surface. Similarly, fiber alignment is assumed to be perfect. The net impact of these assumptions is that for the case of compression in composites, micromechanical theory is generally invalid. The model is too idealistic.

It is emphasized that the microanalysis in the literature to date addresses only static compression. When compressive fatigue of composite materials is the subject at hand, the shortcomings of present micromechanics theory become so great the quantification of the process becomes nigh impossible.

For this reason, no micromechanical analysis is attempted in this study. Rather than use an analytical approach to the problem, a systematic experimental approach addressing the empirical differences of varying geometrical parameters within fixed fiber-matrix systems is utilized.

D. Predominant Failure Mechanisms

This section presents an overview of the literature pertaining to (1) failure of composites subjected to static compressive loads, (2) failure and damage phenomenon in composites subjected to tensile fatigue loading, and (3) interlaminar shear. The relevance of the first is apparent from the previous section. However, the inclusion of the second and third subjects needs some initial justification. Although it seems highly unlikely that composites react to compressive fatigue as they do to tensile fatigue, it seems that the question must at least be posed: is "Compressive Fatigue" equivalent to "Static Compression" + "Fatigue"? In a phenomenonological sense, it can be speculated that some principle of superposition exists which explains compressive fatigue in composites. Lastly, the mechanism and characteristics of interlaminar shear stress in composites are included because interlaminar shear failure is one of the primary modes of lamina debonding; for every ply that is debonded, the stiffness (EI) of the composite beam is reduced by some discrete amount and the Euler critical load (P_{cr}) is thereby reduced by the same factor (see equation [7]). In effect, the beam becomes "more slender". It can be postulated that in a unidirectional ply composite under compressive fatigue loading there occurs a ply-by-ply debonding which proceeds to discretely reduce the effective area (A) of the beam until the P_{cr} for the reduced beam equals P, the applied load, and

"macrobuckling" occurs (see Chapter 2-B).

Physically, longitudinal compression micrographs show a cleavage type failure which is typical of brittle materials. Broutman (8) gives six modes of longitudinal compressive failure that augment the two basic modes shown in Figure 6:

a) Filament microbuckling, matrix still elastic
b) Matrix yield followed by filament microbuckling
c) Constituent debonding followed by filament microbuckling
d) Panel microbuckling
e) Shear failure
f) Ply separation by transverse tension through the thickness

Fried (10) states that yielding of the matrix is generally the controlling factor - compressive strength is "resin-dominated". The point at which the matrix yields or flows determines the compressive load carrying capacity of the composite. The matrix, in effect, acts to support the fiber under "hydrostatic" pressure; the fiber continues to function as a load carrying member up to the point at which this pressure releases as the matrix yields, following which the fiber buckles, and the composite fails. This concept results in the Rule of Mixtures model of equation [9] and represents a simple, basic model: The resin acts to stabilize the filaments so that the latter can sustain high stresses and failure occurs only when the effectiveness of the resin in providing adequate

support is reduced. The model assumes that each fiber is surrounded by a large volume of matrix and that no bond exists between the fiber and the matrix. Also implicit is the assumption that the matrix is "ductile". In real composite materials each individual fiber is supported not only by matrix but also by adjacent fibers and adjacent plies; the compressive strength of real materials is not as high as that predicted by the model (when the yield stress is reached in the resin). Also, many matrix materials are glassy and brittle.

More realistically, then, a conceptual description of the processes occuring in a composite during static compression would be as follows: the matrix, in conjunction with the bond between it and the fibers, serves to distribute the load among the fibers (which may be of different effective lengths or may be at various angular attitudes). Ideally, each individual fiber is surrounded uniformly by the matrix and other fibers, all of which resist lateral forces and tend to stabilize the fiber and increase its load carrying capacity. However, it is obvious that all bonds cannot be uniform and that the continuity of the matrix is in reality interrupted by voids and inclusions, so that it is likely that failure commences with the failure of a single filament somewhere in the structure, either by buckling if the lateral force developed exceeds the supporting lateral force (i.e. if the fiber is in the close proximity of a void), or at the ultimate compressive stress

of the fiber if the lateral force is sufficiently strong. Thus, the load carrying capacity of the composite may indeed be in the limit determined by the yield point of the matrix, since yielding or flowing of the matrix may lead to the loss of column support and hence catastrophic failure. With the failure of any one fiber in the structure, a discontinuity is formed which may act as a notch, and cracking would thence proceed in the manner characteristic of brittle fracture. This process leads to the conclusion that with other factors such as dimensions and modulus being equal, a matrix of higher yield strength would produce a composite of high compressive strength. Also, the Poisson's ratio of the matrix may be a significant factor in determining the effective lateral support in that a higher Poisson's ratio would imply less support and fiber failure at lower loads. (10)

Factors which may affect the function of the matrix to laterally stabilize the fibers are: (10)

a) The physical properties of the matrix. Although the direct load-carrying capability of the matrix may be small, the matrix yield strength may be of major importance in providing lateral support to the fibers. Other important properties may include matrix stiffness, shear strength and shear rigidity, and tensile strength if buckling of the individual fibers involves a cohesive failure in the matrix.

b) The chemical characteristics of the matrix such as molecular weight and degree and nature of cross-linking.

The degree of bonding with the fibers is especially important.

c) Matrix volume fraction. As opposed to tensile loading, where matrix content is generally minimized (ideally zero), compressive loading demands matrix for the required lateral support. Theoretically, for compressive loading, there should be some optimum resin content, which gives the required lateral support to the fibers without assuming excess load.

Since the fibers are the principle load carriers in the composite, their composition is also obviously of importance. The effectiveness of the fibers is a function of: (10)

a) The nature and characteristics of the basic material, including compressive modulus and strength, shear characteristics, and brittleness. The chemical nature as pertains to moisture absorbtion and reactivity with finishing agents or the matrix is also important for bonding purposes.

b) Geometric factors such as straightness, uniformity of cross-section, and cross-sectional shape and area. It may be desirable to employ fibers of greater diameter.

The addition of fatigue to the compression loading of a composite complicates matters somewhat. Fatigue in general results in cyclic stressing of the molecular bonds of the polymer chains as well as the bonds between matrix and fiber. On the proper scale, fatigue in composites may be considered analogous to fatigue in metals: the formation and propagation of microcracks in the matrix may be compared to the transgranular travel of fatigue cracks which ultimately causes

catastrophic failure in homogeneous structures (12). Tensile fatigue in composites results in cracks arising from slip bands which extend in increasing increments every cycle by accumulation of irreversible plastic distortions of the crack tip, until a critical flaw size is reached (8). The applied load produces large internal stress concentrations. The matrix responds to these concentrations by cracking. Tensile fatigue results in the following physical actions in GRP (McGarry 1969):

1) The damage accumulates as the number of cycles increases, although the effect of the first stress application is disproportionately large.

2) Cracking is most likely in regions of high-fiber density; resin rich areas rarely initiate cracks even when they contain voids.

3) Fibers oriented perpendicular to the applied stress are most likely to produce cracks, while parallel fibers are least likely to do so.

4) Once initiated, the cracks can run parallel to the fibers unless they encounter other fibers spanning the crack path. In this case, the cracks deflect, or terminate if the spanning fiber is nearly perpendicular to the path.

5) The cracking reduces the strength and modulus of the composite, changes its Poisson's Ratio, increases the mechanical hysteresis it displays and increases its absorbtivity to liquids. All of these effects can be used as indices of internal damage.

These microcracks nucleate and extend in increasing increments with each cycle by accumulation of irreversible plastic distortions of the crack tip, until they become large enough to fracture the specimen by rapid propagation "...in a quarter cycle". (8)

The initial imperfections in the composite such as broken fibers, delaminations, matrix cracking, fiber debonding, voids, and inclusions can be much larger than corresponding imperfections in conventional metals, especially when compared to the fiber diameter (i.e. the filament diameter in the graphite composite tested in this study is .0003 inches with 10,000 filaments per "tow"). The growth of damage in metals, however, is typically more abrupt, illustrating the fact that composites are generally less susceptible to the effects of stress concentrations than are metals (see Chapter 5). Composites are similar to metals, however, in the sense that fatigue cracks are encouraged by surface imperfections (9). Surface deterioration, weakened surface laminae zones due to non-uniform matrix material, fiber errors, machining errors, voids, or notches can all be deleterious to fatigue strength.

On a laminar scale, the predominant mode of failure in fatigue in composites is that of shear. The factors usually associated with the fatigue life of GRP in a macro-sense are: (11)

1) Interlaminar Shear
2) Compressive Strength

3) Resin Content

4) Resin Modulus

5) Filament Orientation

6) Macro-void Content

7) Residual Stress

8) Moisture Effects

9) Strain Magnification in the Matrix

10) Interface (glass-to-finish bond)

11) Interface (matrix-to-finish bond)

12) Micro-void Content

The interlaminar shear strength is given by Broutman (8) as

$$S_s = \beta_s(\varepsilon_{ms}/\beta_v\phi)G_s \qquad [13]$$

where

β_s = theory - experiment correlation factor

ε_{ms} = allowable matrix shear strain

β_v = void factor

ϕ = shear matrix - strain magnification factor

G_s = composite shear modulus

Stripped of all the undetermined constants, this equation implies that the interlaminar shear strength, and hence the compressive fatigue strength of the composite, is directly proportional to the shear modulus of the composite.

The existence of interlaminar shear stresses (τ_{xz} in Figure 5) means that the composite can delaminate near free edges whether they be at the edge of the plate, around a hole, or at the ends (9). The interlaminar shear strength is a good measure of the interfacial bond strength.

The interlaminar shear stresses can be affected by the laminate stacking sequence (9). Since progressive delamination is one of the primary failure modes in fatigue, this is very important. Jones (9) gives the following guidelines concerning control of interlaminar shear properties through stacking sequence:

1) $\pm\theta$ laminates exhibit only shear coupling (no Poisson's Ratio mismatch between layers) so τ_{xz} (the interlaminar shear stress) is the only nonzero interlaminar stress.

2) 0°/90° laminates exhibit only a Poisson's Ratio mismatch between layers (no shear coupling) so τ_{yz} and σ_z are the only nonzero interlaminar stresses.

3) Combinations of the above, for example $\pm\theta_1$ and $\pm\theta_2$ laminates, exhibit both shear coupling and Poisson's Ratio mismatch between layers, and so have τ_{xz}, τ_{yz}, and σ_z interlaminar stresses.

The interlaminar shear strength should be maximized in composites designed for use in compressive fatigue loading conditions, hence the conceptually optimum lay-up orientation would incorporate some mix of 0° plies to bear the load with $\pm$45° plies to minimize the interlaminar shear stress (for

uniaxial loading in the 0° direction). Typical advanced laminates used for structural applications are of the $[0_i°/\pm45_j°/90_k°]$ family of orientations. "The 0° direction is generally oriented parallel to the principal axial loading direction; $\pm$45° plies provide shear strength and stiffness or buckling resistance; and 90° plies in $[0_i°/\pm45_j°]$ laminates reduce the Poisson's Ratio, can be used to mitigate some of the free edge stresses, and can result in strength and stiffness benefits depending on the loading direction. However, the 90° plies may crack at a fraction of the ultimate tensile strength of the laminates, complicating the fatigue problem." (12)

E. Effects of Immersion

Composites may be subject to degradation of physical and mechanical properties upon exposure to water. This degradation must be considered when using composites for marine applications, as well as other applications where significant humidity may be present. "Wet" rather than "dry" strengths and modulii must be used in the design of marine structures. The degree of degradation depends on the materials employed, the fabrication quality of the structure, the temperature and chemical composition of the environment, and the loading encountered.

Design criteria for the selection of appropriate factors of safety as related to loss of strength due to immersion are practically nonexistent for composites. Mandell (13) found that for woven roving, chopped strand mat, and scotchply laminates: "A water environment reduces the ultimate tensile strength of unnotched samples for both static and cyclic loading. However, water tends to accelerate cracks under cyclic loading while decelerating them under static loading." Macander and Silvergleit (14) studied the effects of immersion on interlaminar shear (recall its importance to compressive fatigue!) and flexural strength. Expanding on previous indications that the ultimate tensile strength was unaffected by long periods of water immersion while interlaminar shear, flexural, and compressive strengths were all affected to the same degree (and were much more sensitive to water) they came

to the following general conclusions:

1) Maximum degradation occurs during the initial immersion period.

2) Further extended immersion beyond the initial period does not adversely affect composite strength retention.

3) After a 26 week immersion period (at room temperature) water absorbtion varied from .3% to .8% (for various GRP and graphite laminates).

4) The amount of water absorbed does not appear to correlate with strength retention. Factors such as resin composition, degree of cure, hardener selection, and stoichiometry influence the rate of water absorbtion.

5) A well made laminate with a void content less than 1% is not adversely affected by long term immersion in water.

6) Shear strength retention for a 2.5% void content material was approximately 80% for a 12 month immersion period.

7) After 10,000 cycles, the HTS graphite composite sustained over 85% of its initial interlaminar shear strength when tested in air, and 80% of its initial strength when fatigue tested fully immersed.

8) Degradative effects on composites, subjected to steady load or fatigue, are more pronounced when the material is immersed in water.

From these conclusions, we can reasonably expect up to

a 20% downward shift in compressive fatigue curves for the immersed data sets. No information could be found in the literature on how composites react on a molecular scale to compressive fatigue, or of how H_2O might attack the matrix, the fiber, or the interface during this cyclic compression; the only information found is empirical.

Chapter 3

Materials and Test Methods

In addressing the experimental approach to be used in the study of compressive fatigue loading of composites, several conflicting practical considerations had to be reconciled. The basic problem was one of designing a gripping mechanism that would (1) be compatible with the available test equipment and (2) accomodate samples of such dimensions that they would act as "short columns" (of small slenderness ratio) that would characteristically fail due to "materials" reasons rather than as long slender Euler columns (see Chapter 2-B). The basic constraints were (1) the capacity (10,000 lbf) of the testing machine, (2) the maximum and minimum size of the grip compatible with the stroke of the machine (12 inches < grip length < 16 inches), (3) the fact that a "cage" type grip mechanism would have to be employed because the machine was designed for tensile fatigue, and (4) the range of expected stress limits to be used, in order to fix the specimen dimensions. The net result of the process of synthesizing these factors into hardware that would yield relevant data is contained in this chapter.

A. Materials

The materials to be tested were selected to provide a broad variety of marine composite materials. Though necessarily not completely comprehensive, the list chosen is felt to provide a good representation of those glass laminates currently in use and advanced composites that may be applicable to marine applications in the near future. The principle physical properties of all samples are given in Table 2.

A physical description of the materials tested follows:

Polyester Resins

Sample Type 1: Style 61 woven roving (E-glass) with Laminac 4155 (American Cynamid Company) with a .5% MEK peroxide, fabricated by hand lay-up using 18 layers of glass rovings with 600 grams of matrix material, compression molded at .35MN/M^2 and 90°F for 24 hours, and then postcured at 200°F for two hours. Nominal sample size .34 inches x .35 inches x 5.5 inches.

Sample Type 2: Chopped strand mat (1.5 ounces) with Laminac 4155 fabricated as above. Nominal sample size .34 inches x .35 inches x 5.5 inches.

Epoxy Resins

Sample Types 3a,3b,3c: Scotchply Type 1003 unidirectional ply, epoxy matrix (3-M Company) compression molded at 150 psi and 350°F for one hour. Nominal sample size .34 inches x .35 inches x 5.5 inches.

Sample Types 4,5,6,7,8: Union Carbide Thornel 300 graphite filaments with Narmco 5208 epoxy resin, supplied by the David Taylor Research and Development Center, Annapolis, Maryland. Nominal sample size .22 inches x .25 inches x 5.25 inches.

All sample beams were sandwiched with [0°/90°/0°/90°/0°] scotchply tapered tabs at each end, bonded to the surface 0° plies of the samples with epoxy adhesive. These tabs served to effectively concentrate the applied stress in the longitudinal center of the samples rather than at the ends or at the gripping blocks where uncontrollable stress concentrations were expected.

Figure 2 is a schematic of the gripping cage with a sample in place.

B. Test Equipment and Instrumentation

Test specimens were cut on a diamond-edged wet saw to be compatible with the grip (Figure 2). The grip mechanism was designed in a "cage" configuration in order to afford the necessary features of: (1) compatability with the Instron Universal or Model 1211 testing machines, (2) close alignment of specimen to the direction of applied stress, (3) sufficient strength to give a factor of safety of 3 to an applied load of 10,000 pounds (the maximum expected), and (4) uniform stress distribution across the ends of the specimen.

Static compression tests were conducted on the Instron Universal machine. Fatigue testing entailed use of the Instron 1211.

C. Test Procedures

Compressive fatigue failure data were obtained on an Instron Model 1211 dynamic cycler at constant load amplitude with a sinusoidal load versus time at a frequency of 7 Hertz. This low frequency was chosen to avoid heating of the specimen during loading which may have influenced the results. All loading was compression; to avoid slippage or misalignment in the grips during testing, a minimum load of 500 pounds was maintained. A schematic of a typical loading history is shown in Figure 3.

No attempt was made to control the environment in which the tests were conducted. The environment for the dry samples was ambient (approximately 75°F, 50-70% relative humidity). Surface wetness for "wet" samples was maintained by wicking distilled water from a beaker onto the mid-section of the sample with cheesecloth. These "wet" samples were presoaked in distilled water at 180°F for 13 weeks to enhance absorbtion (the absorbtion history during presoak is shown in Figure 4).

D. Data Analysis Procedure

The purpose of the data analysis was to:

1) Determine a quantitative relationship between the cyclic compressive stress level and the number of cycles to failure for each sample type, thereby generating S-N curves.

2) Determine reasonable qualitative relationships, using whatever physical parameters were deemed necessary, to effect statistically relevant relationships between the fatigue resistance of the materials and their other various physical and mechanical properties.

In order to accomplish these two tasks, the MITSNAP data analysis package was utilized. It was assumed that the conditional distribution of maximum applied stress given (logN) was normal with a mean that was a linear function of (logN), and that successive values of (σ - E(σ/(logN)) were independent. The analysis for task (1) above was then limited to Regression Analysis by the method of least squares. All data points with the exception of "run-out" points were used; the endurance limit (if one indeed exists) was not defined by this procedure.

Chapter 4

Results and Discussion

A. Statistical

The results of the curve fitting process are presented in Figures 8 through 15. Figure 16 shows the following rank ordering by stress amplitude of S-N curves:

1) [0°/90°] Graphite
2) [0°/±45°/90°] Graphite
3) [0°/±45°] Graphite
4) [0°/90°] Glass
5) [0°/±45°] Glass
6) [0°/±45°/90°] Glass
7) Woven Roving Glass
8) Chopped Mat Glass

Table 17 presents the statistical results in tabular form.

For the purpose of the Multiple Regression Analysis, only the unidirectional sample data sets (Scotchply 1003 Glass and T300/5208 Graphite) were used. Following the theories addressed in Chapters 2-C and 2-D, it was postulated that, for a first approximation, the number of 0° plies in a sample should statistically "explain", along with the applied stress, the compressive fatigue resistance of that sample. For this analysis, the dependent variable was the number of cycles to failure and the explanatory variables were the stress level and the number of 0° plies in each sample. To measure the

statistical correlation among these variables, the first iteration of the Multiple Regression Analysis utilized only the three graphite configurations aggregated together as a sample set. The results were disappointing: (1) $R^2 = .4678$, or the proportion of the total variance in log(N) explained by the regression equation was very low, and (2) the correlation of the number of 0° plies is only 0.0491, indicating that compressive fatigue resistance is barely dependent at all on the number of 0° plies (relative to the applied stress).

Next, the Regression was performed on log(N) versus applied stress, number of 0° plies, number of 90° plies, and number of $\pm$45° plies for each data point. The same aggregated sample set was used. The results: (1) $R^2 = .7242$, or the explanation of variance was improved considerably, although still very low by statistical standards, and (2) the correlation values obtained were

Stress = -0.5459

Number of 0° plies = -0.0491

Number of 90° plies = -0.0555

Number of $\pm$45° plies = -0.0583

These values indicate that the fatigue resistance of the different ply orientations are correlated, in decreasing order, to the applied stress, the number of $\pm$45° plies, 90° plies, and 0° plies respectively. However, one of the data subsets

(Sample 4) contained no ±45° plies and another (Sample 5) contained no 90° plies. Conceptually, the analysis becomes confusing and of questionable relevance: the high value of the ±45° ply coefficient indicates that the number of these plies present in a sample is more important than the number of 0° plies. Since the ±45° plies are not load-bearers (to the degree that the 0° plies are) one has to wonder about the validity of the analysis. The physical explanation for this is probably that the number of ±45° plies is directly related to the shear strength of the material, which has been shown (Chapter 2) to be one of the controlling parameters in compressive strength.

It is evident that at least one further iteration of the Regression was necessary; there were obviously other, more important parameters controlling the compressive fatigue resistance of these materials than just the stacking sequences. In order to make this step of the analysis as general as possible while remaining sufficiently succinct to enable specific statistical conclusions to be drawn, it would be necessary to aggregate all of the unidirectional ply data (both glass and graphite) into a single set, and then explain log(N) as a function of the following physical and mechanical parameters:

1) Applied stress, σ
2) % 0° plies in specimen
3) % 90° plies in specimen

4) % $\pm$45° plies in specimen

5) Shear Modulus of the specimen, G

6) Ultimate Compressive stress of the specimen, σ_{ult}

7) The Compressive value of Young's Modulii for the specimen, E_f and E_m

8) Poisson's Ratio for the specimen, v

There are two subsets of these parameters that are coupled: first, as has been stated, the percentage of $\pm$45° plies in a sample is probably very indicative of the shear strength of the sample (and hence G) and second, the static strength of the material, σ_{ult}, is directly related to ultimate strain of the material by Young's modulus (Hooke's Law), if the material is assumed to be elastic. These couples would cause nonlinearities (at best) and statistical nonsense (at worst) in the reduction of the data and hence one parameter out of each couple would have to be removed to add credence to the regression equations obtained. Which parameters to exclude would be arbitrary; the net result would be that the equations obtained would be of the basic form:

$$\text{Log}(N) = a(\sigma) + b(\%0°) + c(\%90°) + d(\%45°) + e(\sigma_{ult}) + f(v) \qquad [14]$$

where

a,b,c,d,e, and f are constants

Deviations from this empirical formula would be due to all of the other critical factors stated in Chapter 2, specifically:

1) any misalignment of the sample
2) any surface or edge defects
3) the void content of the sample
4) interlaminar stresses and strains
5) any macro-voids or inclusions
6) sensitivity of physical properties to fabrication quality control
7) fiber-matrix bond strengths

In view of this impressive list, it was decided that the refined quantification of the compressive fatigue phenomenon gained by the use of multiple regression would be, at best, of very questionable worth, even if a high R^2 happened to be obtained. This method of analysis was therefore abandoned in favor of the following simple methodology: the characteristics of the S-N curves (i.e. slopes and intercepts) of the various samples would be ranked and compared in a tabular format with various physical properties, and general conclusions drawn. In consonance with the "Percentage of Ultimate" concept wherein the applied fatigue stress is expressed as a percentage of the ultimate static stress to predict the fatigue life, the comparison was accomplished by independently ranking and investigating the stress axis intercepts (indicative of static compressive failure) and the slopes (indicative of how each

sample type reacts to fatigue loading). The intercept comparison matrix is contained in Table 18, and the slope comparison in Table 19.

Viewed exclusively from a statistical perspective, the following list of conclusions and observations is presented concerning the phenomenon of compressive fatigue in composites:

1) The S-N curves for all specimen types and configurations show a linear relationship between maximum applied stress and the logarithm of the number of cycles to failure for the range of stresses imposed. For the model and method of regression used, the Coefficients of Correlation varied from a low of -.827 (for chopped mat) to a high of -.978 (for wet T300/5208 [0°/$\pm$45°]).

2) All specimen types may reach an endurance limit indicating infinite fatigue life under a critical "lower bound" stress, however this was not shown. For the purposes of curve-fitting, data which were considered "run-outs" after about 10^6 cycles were not included in the regression.

3) A "normalized slope" parameter was used to characterize the fatigue resistance of a material independently of its static compressive strength. The slope of each S-N curve was normalized to its' intercept (which is, theoretically, the stress at 1 cycle, or the static compressive strength). The results are tabulated in Table 19. Three conclusions can be drawn: the first is that, in general, the graphite composites show better compressive fatigue resistance than do

the glass composites, and the second is that composites show better fatigue resistance in compression than in tension. Figure 17 shows this relationship graphically. The relatively high apparent fatigue resistance of the woven roving and chopped mat laminates relative to the advanced glass and graphite composites is an unexpected result. The relatively high void contents and "disorder" of these composites would seemingly relegate them to the bottom of the list. Within the limits of accuracy of this analysis it can reasonably be stated that the T300/5208 system is "better" from a fatigue resistance standpoint than any of the glass systems tested. The third conclusion is that statistically it is consistent to state that "compressive fatigue" is equivalent to "static compression" superimposed with "fatigue".

4) Environmental degradation from distilled water of the T300/5208 is present. A small downward shift of the S-N curve is noted; for the [0°/$\pm$45°] orientation the normalized slope increased by 4.9% and the static strength decreased by 9.1%, and for the [0°/$\pm$45°/90°] orientation the normalized slope increased by 16.3% while the static strength decreased by 5.1%. From these figures it can be concluded that degradation of fatigue strength "on the order of" 10% occured due to the soak. This is in rough agreement with the Macander-Silvergleit conclusion in Chapter 3-E. Especially notable is the absence of wet [0°/90°] data: all samples tested, even at very low applied loads, failed by end crushing, and hence were unattainable.

5) 95% Confidence Levels are included in Figures 8 through 15. The lower bound represents a design stress to be used for a 95% "Confidence Level" that the material will not fail given a specified total number of cycles whereas the upper bound represents a 95% Confidence Level that the material will fail at the specified number of cycles. The width of the band is representative of the scatter of the data as embodied in the standard deviation of each data set (see Table 17). The validity of these Confidence Levels is therefore dependent on the sample size, since in general a larger sample size yields more valid statistical results when a normal distribution is assumed. A set of at least thirty data points is normally required; due to time constraints, some of the data sets used in this analysis contain as few as twelve points, and therefore the statistical validity of the results must be viewed with some skepticism.

6) Table 18 (Intercept Comparisons) indicates that the T300/5208 high strength graphite composites show the greatest compressive strength, followed by the undirectional scotchply glass, the woven roving glass, and the chopped mat glass. On the basis of general strength, modulus, and geometrical considerations, this ranking is what would be expected. Note in Table 18 that the rank ordering by compressive strengths does not correlate with the rank ordering by tensile strengths, particularly in the case of the [0°/$\pm$45°] and [0°/$\pm$45°/90°] graphite laminates. The implication of this fact is that the

presense of the 90% plies in the "weaker" (tensile strength) [0°/±45°/90°] laminate may cause it to be stronger in compression than the [0°/±45°] configuration.

7) Given a unidirectional composite system, the [0°/90°] configuration is the strongest in compression. This result might also be expected, since the percentage of 0° "load-bearing" plies is higher in this type of lay-up. For the T300/5208 system, the compressive strengths of [0°/±45°/90°] and [0°/±45°] orientations are within 1.3% of each other, while for the glass system, the [0°/±45°] system is clearly stronger than the [0°/±45°/90°] system. Note that the [0°/±45°] laminates have 8% more 0° plies than the [0°/±45°/90°] laminates; obviously some factor other than the percentage of 0° plies is of consequence.

8) It is of interest to note that the largest physical property difference in the unidirectional glass and graphite laminates is in the fibers: the ultimate strain of E-glass is an order of magnitude higher than that for Thornel 300 graphite fibers.

	E-Glass	T-300
Strength	500×10^3	300×10^3
Modulus	10×10^6	50×10^6
Ultimate Strain	.05	.006

Since both composites have epoxy matrices, any significant differences in macro-strength properties could be rationalized in terms of this large difference in ultimate strain. The

most obvious consequence of this difference is that the interlaminar shear strain (and hence stress) will be much higher for the E-glass material, since 0° plies will "slide" or "slip" more (relative to cross-plies) than in the case of the graphite material during each stress cycle. This concept of the stiffness of the fibers being of importance to the compressive fatigue resistance of composites is at odds with the idea that the phenomena is "resin dominated". However, it does merit further investigation. In advanced unidirectional laminates where the fiber volume fraction is .75 or more, the resin may in fact be of little relative importance to the compressive fatigue resistance other than in its function of adhering adjacent laminae (where its shear strength is very important). The ideal materials for compressive fatigue resistance would then be fibers of maximum stiffness with a matrix of maximum shear strength.

B. Physical

Photographs of typical failed specimens are contained in Figures 18 through 26. In general, the glass composites appeared to fail in the shear mode, while the graphite composites appeared to fail in the panel buckling, or "extensional" mode (refer to Figure 6). Contrary to the notion that any given system will fail in either or both modes (depending on the applied stress and fiber volume fraction), this study seems to indicate that the mode of buckling is controlled by the physical system characteristics (E_m,E_f,ν,G_m,etc.) regardless of stress level and is therefore predetermined from a design perspective for a particular application simply by material selection. The fact that the graphite laminates are generally more fatigue resistant than the glass unidirectional laminates may in part be due to the mode of buckling that happens to occur. The implication of this observation is that a system such as the unidirectional glass system could show a significant increase in fatigue resistance if the mode of failure could be changed from shear to extensional by judiciously altering E_m,G_m, and E_f.

Other "macro" physical observations concerning the compressive fatigue of the sample sets tested are:

1) Composite beams buckle in an Euler column fashion: a critical value P_{cr} is reached where the column becomes unstable and buckles. The test is extremely sensitive to misalignment; specimens failed at significantly lower loads when

misaligned slightly. Note in Table 16 that not all specimen types can be classified as "short" columns. All unidirectional glass and two unidirectional graphite samples are, by nature of their dimensions, "intermediate" columns, albeit nearly "short". This calculation is sensitive to the geometrical value assumed for the effective length and the effective width of the specimen h; if ℓe was taken as $.3\ell$, for example, all of the columns would have been "short". Also, all of these columns are close enough to the break point of the curve in Figure 7 that outer ply delaminations caused by fatigue mechanisms would indeed make them "more slender" and hence more susceptible to Euler buckling.

2) The mechanism with which a P_{cr} is reached during cyclic compressive loading appears to be a successive shrinkage of effective cross-sectional area of the beam by delamination of the outer plies so that the nominal stress approaches the critical buckling stress of the material.

3) Failure of the specimens was immediate and catastrophic when it did occur, in the manner of unstable fracture. Rather than "buckle", a more descriptive phrase would be that the specimens "suddenly crush".

4) Ultimate failure appearances indicate than panel (or plate) microbuckling is the mode in which catastrophic failure occurs.

Micrographs of pre-failure damage in "run-out" samples are contained in Figures 27 through 34. The micro-

graphs indicate that outer ply debonding results from cracks initiated at the corners of the specimens. These cracks appear to occur only in the matrix material, and result in major interlaminar cracks and subsequent debonding. No cracks initiating from the flat sides of the specimens were observed.

Specific comments concerning each micrograph are as follows:

Figure 27: A crack initiating in a transverse (90°) ply in a [0°/90°] glass laminate illustrates the compressive fatigue weakness of this lay-up in the z direction. This crack was probably caused by cyclic transverse Poisson's Ratio strain in conjunction with the obvious surface roughness of the specimen.

Figure 28: This major debonding crack occurs at the interface between the outer 0° ply and the adjacent $\pm$45° ply of a [0°/$\pm$45°/90°] glass laminate. Note that there appears to be a row one or two fibers thick of 45° fibers on the 0° side of the crack; the crack is not at the exact interface of the laminae.

Figure 29: The outer two plies of this [0°/$\pm$45°/90°] glass specimen have debonded. Note the incipient crushing and loss of integrity of the debonded plies as compared to Figure 28.

Figures 30 and 31: Major debonding cracks initiating at the corner interfaces of the 0° and 45° laminae of a [0°/$\pm$45°] graphite specimen are illustrated. Note that the

cracks do not exactly follow the interface, and that in fact the crack in Figure 31 does not propagate along the interface (which would ultimately result in debonding) but rather returns to the surface of the specimen.

Figure 32: This corner crack in a [0°/±45°/90°] graphite specimen supports the observation made above: although cracks initiate at the corners, they do not necessarily always result in interlaminar cracks and subsequent debonding.

Figures 33 and 34: Although no cracking is evidenced in these micrographs, they illustrate an interesting defect found in one of the [0°/±45°/90°] graphite specimens. What are apparently resin-rich voids appear near the ends of some of the 0° laminae. This defect was found only in this particular specimen and is indicative of a typical error in fabrication: if care is not taken to insure the transverse integrity of the preimpregnated pliable sheets of unidirectional fibers during lay-up, in situ resin rich areas will result in the finished composite. This type of error is obviously deleterious to the mechanical and physical integrity of the material.

In summary, the observable phenomena that manifested themselves during the tests that comprised this study tend to support the published information concerning the failure mechanisms and characteristics as reviewed in Chapter 3. These observations indicate that the compressive fatigue resistance of composites can probably be improved by:

1) Improving the crack resistance of the matrix

2) Polishing, binding, or cladding the specimens to prevent outer ply delamination and reduce the surface roughness which initiates cracks

3) Use unidirectional composites rather than roving or mat composites. When unidirectional systems are utilized, increase the percentage of 0° plies.

The actual micromechanism that causes fatigue failure was not established. Although it appears from the micrographs to be matrix cracks initiating from the corners, this phenomena is more a result of specimen geometry than matrix or fiber behavior. According to this perspective, the fatigue life at any stress less than the ultimate compressive stress would be infinite if the specimen morphology was such that no free edge stresses or surface roughness existed.

Chapter 5

Recommendations

1) Accumulate more data to verify the statistical results, specifically the Confidence Levels obtained.

2) Conduct low-cycle and high-cycle fatigue tests to verify the "percentage of ultimate" concept and to investigate the possibility of endurance limits of composites.

3) Conduct tests of various other stacking sequences of the $[0_i°/\pm45_j°/90_k°]$ unidirectional laminate family to establish a practical optimum lay-up. Figure 17 and Table 19 indicate that the optimum lay-up would contain plies in all three directions, but with a higher percentage of 0° plies than the laminates used for this study. For example, Lockheed has offered the following "optimum" lay-up sequence for compressive fatigue resistance:

$$[0°/+45°/0_2°/-45°/0_2°/+45°/0_2°/-45°/0_2°]s$$

This scheme is based on the notion that separating the +45° plies from the -45° plies reduces the interlaminar normal stresses compared to laminates that have the +45° and -45° plies adjacent. This laminate contains 67% 0° plies.

4) Investigate the actual micromechanisms of fatigue failure in composites. Parametric studies varying fiber and matrix modulii and strengths, the Poisson's Ratio and the notch toughness of the matrix, and fiber-matrix bonding agents should be conducted to identify and isolate the controlling

factors.

5) Conduct studies on the effects of banding or cladding the specimens to prevent surface crack deterioration by ameliorating surface imperfections and free edge stresses. Another alternative for test methods which avoid these factors may be to use a thin walled tube for specimen geometry.

6) Examine the effects of fiber geometry such as increased fiber diameter or the use of hollow fibers.

7) Conduct reverse-stress cyclic fatigue tests at varying moderate tensile stress levels to determine the effects of small amounts of tensile fatigue on the overall compressive fatigue resistance of these materials.

8) Conduct exhaustive pre-failure microscopy studies. The sudden manner with which ultimate failure occurs and the large scatter in data obtained make it extremely difficult to determine the appropriate point at which to terminate loading in order to obtain meaningful pre-failure damage micrographs, but the nature of fatigue damage in these materials will not be fully understood until significant pre-failure microscopic damage evidence is obtained.

References

1. J. Bader, "Potential Applications of Advanced Composites to High Performance Ship Structures", Naval Ship Research and Development Center, Bethesda, Maryland, 1975.

2. L.B. Greszczuk and A.V. Hawley, "Applications of Advanced Composites to Patrol Craft Hydrofoils", McDonnell Douglas Astronautics Company, Huntington Beach, California, 1973.

3. L.B. Greszczuk and A.V. Hawley, "Application of Advanced Composites to Hydrofoil Strut", McDonnell Douglas Astronautics Company, Huntington Beach, California, 1973.

4. S.P. Timoshenko and J.M. Gere, Theory of Elastic Stability, McGraw-Hill Book Company, New York, 1961.

5. J.P. Den Hartog, Advanced Strength of Materials, McGraw-Hill Book Company, New York, 1952.

6. W.D. Pilkey and O.H. Pilkey, Mechanics of Solids, Quantum Publishers, Inc., New York, 1974.

7. A.G.H. Dietz, Composite Engineering Laminates, The M.I.T. Press, Cambridge, Massachusetts, 1969.

8. L.J. Broutman, ed., Composite Materials, Volume 5, Fracture and Fatigue, Academic Press, New York, 1974.

9. R.M. Jones, Mechanics of Composite Materials, Scripta Book Company, Washington, D.C., 1975.

10. N. Fried, "Role of Resin in Reinforced Plastics", Modern Plastics, September, 1963.

11. J.F. Freund and M. Silvergeit, "Fatigue Characteristics of Filament GRP", Modern Plastics, November, 1966.

12. "Ascertainment of the Effect of Compressive Loading on the Fatigue Lifetime of Graphite Epoxy Laminates for Structural Applications", Lockheed-California Company, Air Force Materials Laboratory Report No. V-TR-76-241, December, 1976.

13. J.F. Mandell, et.al., "Effect of Water on the Crack Propagation Rate in Fiberglass Laminates Under Static and Dynamic Loading", M.I.T. Report No. MITSG 75-18.

14. A. Macander and M. Silvergeit, "The Effect of the Marine Environment on Stressed and Unstressed Graphite/Epoxy Composites", Naval Engineers Journal, Vol.89, No.4, August, 1977.

15. Advanced Composites Design Guide, Air Force Flight Dynamics Laboratory, Wright-Patterson Air Force Base, Ohio, 1975.

16. K. Masubuchi, Materials for Ocean Engineering, The M.I.T. Press, 1972.

17. A.S. Argon and F.A. McClintock, ed., Mechanical Behavior of Materials, Addison-Wesley Publishing Company, Reading, Massachusetts, 1966.

18. J.F. Mandell, "Fatigue Crack Propagation in Woven and Non-Woven Fiberglass Laminates", M.I.T. Department of Civil Engineering Report R74-21, April 1974.

Appendix

Economic Comparison with Marine Metals

The economies resulting from the use of composite materials in structures derive from the fact that they have high strength-to-weight ratios; in situations where a vehicle is required to propel a high value payload at a high velocity it is desireable to make the vehicle as light as possible in order to concurrently maximize the payload carrying capacity and velocity-to-installed horsepower ratio. The application of advanced composites to aerospace vehicles is an obvious result of this high strength-to-weight ratio property.

Because of the processes involved in manufacturing composites and the cost of the raw materials needed, the cost per pound of advanced composites has been substantially higher than the costs of structural metals. As a design parameter for "high-performance" vehicles such as the aerospace applications mentioned above, cost has become an important, and at times constraining factor. In commerical marine vehicles the cost of advanced composites is restrictive; it is not likely that fiberglass bulk ore carriers will make their debut in the foreseeable future.

The weight criticality of dynamic lift marine vehicles, however, enables composite materials to become viable alternatives to high strength metals in terms of performance, cost, and produceability. The decision on which material is the

most cost-effective for any given vehicle should be based on the following factors:

1) The serviceability of the material as embodied in its physical characteristics: its strengths,modulii, fatigue resistances, and marine degradation resistance.

2) The weight of the material needed to resist the design loads (specific strength).

3) The cost of the material needed to resist the design loads.

4) The value premium placed on the performance of the vehicle (e.g. how many dollars is it worth to be able to transport fifty automobiles across the English Channel on a hovercraft ferry in 30 minutes rather than on a conventional ferry in two hours, or for that matter, through a tunnel that cost $4 billion, in 20 minutes).

The first three of these factors are readily quantifiable, whereas the fourth, in the case of high performance craft, is very subjective. As stated previously, the primary advantage of "high performance" marine vehicles is speed. How does one put a dollar value on an hour and a half savings in time to transport one's automobile across the English Channel? The value would vary depending on whether one was spending a leisurely weekend, or delivering an urgently needed medicine (in which case an airplane would be faster than a hovercraft).

The design application for which advanced composites seems to be most promising is in the structures of small Naval patrol

craft, where high speed can be crucial. Since the design requirements of such military craft are often couched in terms of transporting a given weapon (the payload) over a specified endurance range at a specified speed, the most expedient method of measuring the "cost-effectiveness" of such a family of vehicles would be to compare the maximum speeds and ranges obtainable given the fixed payload. The problem of choosing a dollar value for the payload is thereby avoided. The weight saved by the utilization of composites can then be utilized for one of two purposes:

1) It can be used for additional fuel, which would increase the range of the vehicle at a given speed (for a geometric replica).

2) A smaller, lighter vehicle can be produced to carry the same payload at a higher speed for the same range, given a fixed propulsion system. The buoyancy or lift gained by the reduction in displacement of the original vehicle can be forgone, leaving a vehicle of smaller displacement.

The methodology to conduct such a comparison basically involves a cost/weight trade-off analysis that compares the cost-to-specific strength ratios of different marine applicable materials. This cost comparison should not be attempted until the preliminary design of the vehicle has proceeded to the point where its structural design has been developed by stress analysis, weight and moment analysis, and where the overall conceptual geometry and scantlings have been arrived at. For

the base case vehicle, quenched and tempered low carbon structural steel will be assumed throughout. The structural weight of a hydrofoil or a Surface Effect Ship, is normally from 50-60% of the total vehicle displacement, so the weight saved by utilizing higher strength/weight ratio materials than structural steel (which gives "value" in the form of enhanced speed, endurance or payload) is balanced in a parametric manner with the increased cost of the material used. The cost per specific strength parameter embodies, then, not only the materials cost, but also the value, in a relative sense of the efficiency of the material in the structure. It's units are dollars/pound/inch, or cost per pound per unit length of structure. This derives from the specific strength of the material, which represents the length of structure of unit cross-sectional area obtainable from one pound of material at its UTS. A longer member (and thence "more structure") can be made from one pound of a material with a high specific strength than can be made from one pound of a material with a lower specific strength, given that the design load for both structures is the same. When the resulting produce is normalized to the cost/specific strength of the base case structural steel, a ranking can be made of the "cost-effectiveness" of the materials. This ranking then indicates which material is the most fiscally attractive. The normalized cost/specific strength factors can then be multiplied by the estimated gross cost of the low carbon Q and T steel structure to give a

final dollar figure which can be used in a judgemental trade-off with the decision makers notion of the value of the weight savings in terms of added endurance (which can be calculated exactly from the fuel weight gained) or enhanced speed (which requires a completely new, if similar, design using the selected advanced material), or payload (which can be in terms of added missiles, torpedoes, etc.).

Table 20 contains a tabulation of the results of comparing the materials used in this study with typical steel, aluminum, and titanium alloys currently used in high performance naval vehicles. For the purposes of this thesis, the comparison is based on the specific ultimate tensile strength of the materials only. The methodology, however, is sufficiently general so that any number and mix of physical and mechanical properties can be used as bases for comparison. The tabulation can easily be expanded: column two of Table 20 can represent any physical or mechanical property of the material such as (but not exclusively) those in the following list:

1) Ultimate compressive strength
2) Tensile fatigue life at a specified number of cycles
3) Compressive fatigue life at a specified number of cycles
4) Tensile or compressive modulii
5) Shear strength or modulus
6) Erosion or corrosion resistance

The analysis would then proceed in exactly the same manner as has been done here, using instead of "specific strengths",

"specific modulii" or "specific fatigue resistances". A different rank ordering will be obtained for each analysis (one list for each property used). These lists can then be weighted to meaningfully reflect the expected loading and environment. The material with the lowest overall cost to "Specific Property Mix" ratio would then be the logical choice.

This method can be used in any materials selection process where cost and weight are the two primary parameters. The method is exact; with the exception of the subjective assignment of Fabrication Figures of Merit and the choice of which physical properties to use, no judgemental decisions need be made concerning the materials. As long as the data used for costs, strengths, modulii, and other properties are valid, the method will yield a logical and proper result.

It is important to realize the limitations of the method, however, and to keep them in mind when making the decision as to which material to use. The major limitation is simply that it is nearly impossible to include all the unique physical and mechanical properties of each and every material: the sheer immensity of the tabulations required would render the results meaningless, and the unique sets of properties of each candidate material may be so different as to preclude meaningful comparison. For example, the corrosive properties of powdered graphite that may have to be contended with in the electrical and other metal-containing subsystems of a vehicle with a T300/5208 structure do not have an analog in vehicles

with metal structures, however the graphite and glass composite structures will not themselves corrode in a marine environment, as will the metals. The chemical characteristics cannot easily be quantified.

The point to be made is very simply this: although advanced composites are fascinating materials from an engineering point of view, the designer or user of these materials must take care not to be blinded by the impressive list of good properties that they possess. Although they have Specific Strengths and Specific Modulii an order of magnitude higher than most other structural materials, they also have other specific properties deriving from their chemical constituents and their morphologies that may make them less desireable for many applications than may at first seem apparent. Most importantly, the engineer should not limit himself to simply filling out the columns of the "Cost-Effectiveness Table" and delivering it to the decision-maker.

TABLE 1

Fiber Volume Fraction, and Ply Thickness

Reinforcement or Material	Nominal Ply Thickness	Nominal Fiber Volume Fraction
Woven Roving	0.020	0.40
Chopped Mat	0.036	0.20
Scotchply	0.010	0.50
T300/5208	0.006	0.63

TABLE 2

Compressive Strength and Stiffness Properties

Specimen	E_c(15,18)	σ_{ult}(Table 18)
Woving Roving	2.2	37,400
Chopped Mat	1.2	23,740
[0°/90°] Glass	2.7	66,130
[0°/$\pm$45°] Glass	2.65	57,590
[0°/$\pm$45°/90°] Glass	2.22	47,123
[0°/90°] Graphite	9.5	113,720
[0°/$\pm$45°] Graphite	9.32	78,300
[0°/$\pm$45°/90°] Graphite	7.81	79,350

TABLE 3

Data for Sample No.1: Glass Woven Rovings

Maximum Applied Stress	Number of Cycles to Failure
22,267	82,820
22,634	56,460
23,346	20,350
23,530	10,580
23,904	11,430
25,591	4,090
26,316	5,000
27,083	9,800
28,000	4,360
28,226	2,370
28,689	1,000
29,046	3,070
30,364	1,030
30,612	190
31,250	280
34,370	1
20,576	2,050,000 Runout
20,661	1,110,000 Runout

TABLE 4

Data for Sample No.2: Glass Chopped Mat

Maximum Applied Stress	Number of Cycles to Failure
14,840	12,420
15,643	1,330
15,979	55,170
16,470	7,380
16,818	4,250
17,720	730
18,315	480
18,667	220
19,677	160
35,300	1
13,062	510,000 Runout
13,990	530,000 Runout

TABLE 5

Data for Sample No.3a: Unidirectional Glass Fibers [0°/90°]

Maximum Applied Stress	Number of Cycles to Failure
28,112	1,684,400
35,311	25,410
35,501	780,000
35,605	173,570
35,712	632,250
36,572	274,000
37,311	187,720
42,508	5,520
43,766	5,190
48,182	5,370
49,777	540
51,905	890
52,210	350
56,999	310
34,304	1,209,600 Runout
33,220	2,053,610 Runout

TABLE 6

Data for Sample No.3b: Unidirectional Glass Fibers [0°/±45°/90°]

Maximum Applied Stress	Number of Cycles to Failure
25,357	90,460
25,362	420,500
34,111	2,810
34,821	3,260
28,251	6,180
29,499	3,390
30,377	99,370
26,116	536,540
30,646	7,520
36,554	750
36,347	1,770
36,570	450
25,362	520,500 Runout

TABLE 7

Data for Sample No.3c: Unidirectional Glass Fibers [0°/±45°

Maximum Applied Stress	Number of Cycles to Failur
58,135	1
58,189	1
44,412	360
35,984	1,370
37,473	1,410
31,579	4,580
29,006	16,200
29,472	198,000
29,491	942,980 Runout
29,025	567,000 Runout

TABLE 8

Data for Sample No.4: Dry T300/5208 [0°/90°]

Maximum Applied Stress	Number of Cycles to Failure
74,372	28,499
75,546	49,440
76,840	14,350
78,989	38,890
90,046	7,710
96,265	50
98,857	40
114,045	450
114,508	1
54,246	1,971,720 Runout
66,215	1,125,350 Runout
68,075	1,066,930 Runout

TABLE 9

Data for Sample No.5: Dry T300/5208 [0°/±45°]

Maximum Applied Stress	Number of Cycles to Failure
45,480	66,670
45,537	84,000
46,142	731,250
52,143	16,670
53,133	160
55,236	11,180
55,745	5,360
62,583	360
64,738	100
66,040	60
76,453	1
37,533	1,100,950 Runout
36,454	937,000 Runout

TABLE 10

Data for Sample No.6: Dry T300/5208 [0°/±45°/90°]

Maximum Applied Stress	Number of Cycles to Failure
55,236	117,660
59,887	50,180
61,274	30,550
61,428	330
69,343	290
70,828	30
71,685	110
47,327	960,000 Runout
51,827	1,231,780 Runout

TABLE 11

Data for Sample No.7: Wet T300/5208 [0°/±45°]

Maximum Applied Stress	Number of Cycles to Failure
64,516	20
64,478	10
55,666	130
54,681	180
46,455	26,420
46,729	6,200
41,336	545,460 Runout

TABLE 12

Data for Sample No.8: Wet T300/5208 [0°/±45°/90°]

Maximum Applied Stress	Number of Cycles to Failure
35,828	544,000 Runout
43,703	425,740
54,181	68,340
51,026	65,230
60,971	5,390
63,892	40
60,892	3,550

TABLE 13

Stacking Sequence for [0°/90°]

Ply No.	Orientation	Ply No.	Orientation
1	0°	23	0°
2	90°	24	90°
3	0°	25	0°
4	90°	26	90°
5	0°	27	0°
6	90°	28	90°
7	0°	29	0°
8	90°	30	90°
9	0°	31	0°
10	90°	32	90°
11	0°	33	0°
12	90°	34	90°
13	0°	35	0°
14	90°	36	90°
15	0°	37	0°
16	90°	38	90°
17	0°	39	0°
18	90°	40	90°
19	0°	41	0°
20	90°		
21	0°		
22	90°		

TABLE 14

Stacking Sequence for [0°/±45°/90°]

Ply No.	Orientation	Ply No.	Orientation
1	0°	23	+45°
2	+45°	24	90°
3	-45°	25	0°
4	90°	26	-45°
5	0°	27	+45°
6	+45°	28	90°
7	-45°	29	0°
8	90°	30	-45°
9	0°	31	+45°
10	+45°	32	90°
11	-45°	33	0°
12	90°	34	-45°
13	0°	35	+45°
14	+45°	36	90°
15	-45°	37	0°
16	90°	38	-45°
17	0°	39	+45°
18	+45°	40	90°
19	-45°	41	0°
20	90°		
21	0°		
22	-45°		

TABLE 15

Stacking Sequence for [0°/±45°]

Ply No.	Orientation	Ply No.	Orientation
1	0°	23	-45°
2	+45°	24	+45°
3	-45°	25	0°
4	0°	26	-45°
5	+45°	27	+45°
6	-45°	28	0°
7	0°	29	-45°
8	+45°	30	+45°
9	-45°	31	0°
10	0°	32	-45°
11	+45°	33	+45°
12	-45°	34	0°
13	0°	35	-45°
14	+45°	36	+45°
15	-45°	37	0°
16	0°	38	-45°
17	+45°	39	+45°
18	-45°	40	0°
19	0°	41	-45°
20	+45°	42	+45°
21	-45°	43	0°
22	0°		

TABLE 16

Stresses in Columns (6)

Specimen	Compressive Modulus	$\sigma_{p\ell}$	$(\ell e/r)_1^*$	$(\ell e/r)_2^{**}$	Type Column (Figure 7)
Woven Roving	2.2	37,400	24.0	22.0	Short
Chopped Strand Mat	1.2	23,740	22.3	22.0	Short
Scotchply:					
[0°/90°]	2.7	66,130	20.1	22.0	Intermediate
[0°/±45°]	2.65	57,590	21.3	22.0	Intermediate
[0°/±45°/90°]	2.22	47,123	21.5	22.0	Intermediate
Graphite:					
[0°/90°]	9.5	113,720	28.7	29.2	Short
[0°/±45°]	9.32	78,300	34.3	29.2	Intermediate
[0°/±45°/90°]	7.81	79,350	31.2	29.2	Intermediate

* $\frac{\ell e}{r} = \sqrt{\frac{\pi^2 E}{\sigma_{p\ell}}}$, the limiting value for the material type

** $r = h/\sqrt{12}$; $\ell e = .4\ell$

TABLE 17

Least Squares Curve Fitting Statistics

Sample	Slope	Intercept	σ_s^2	1.65 σ_s^2= 95% C.L.	Coeff of Correlation
Woven Roving	-3,030	37,400	3,044	5,023	-.927
Chopped Mat	-1,930	23,740	1,567	2,586	-.827
Scotchply [0°/90°]	-5,500	66,130	8,504	14,032	-.943
Scotchply [0°/±45°/90°]	-3,930	47,123	4,479	7,390	-.842
Scotchply [0°/±45°]	-6,219	57,590	12,028	19,846	-.976
Graphite [0°/90°]	-7,530	113,720	16,029	26,448	-.855
Graphite [0°/±45°]	-6,520	78,300	7,775	12,829	-.879
Graphite [0°/±45°/90°]	-4,380	79,350	6,345	10,469	-.885
Wet Gr. [0°/±45°]	-6,222	71,167	9,899	16,333	-.978
Wet Gr. [0°/±45°/90°]	-4,828	75,228	10,145	16,739	-.950

TABLE 18

Intercept Comparisons

Rank	Specimen	Intercept (psi @ 1 cycle)	E_C (msi)	Ultimate Strain	Tensile Strength (psi)
1	[0°/90°] Graphite	113,720	9.5	.0120	105,000
2	[0°/±45°/90°] Graphite	79,350	9.3	.0085	60,000
	Wet [0°/±45°/90°] Graphite	75,228			
3	[0°/±45°] Graphite	78,300	7.8	.0010	73,000
	Wet [0°/±45°] Graphite	71,167			
4	[0°/90°] Glass	66,130	2.7	.0245	61,000
5	[0°/±45°] Glass	57,590	2.65	.0217	
6	[0°/±45°/90°] Glass	47,123	2.22	.0212	
7	Woven Roving	37,400	2.2	.0170	52,000
8	Chopped Mat	23,740	1.2	.0198	25,000

Modulii and Tensile Strength are obtained from (18) and (15)

TABLE 19

Slope Comparisons

Rank	Specimen	Slope (psi/decade)	Normalized Slope (% σ_c/decade)	Normalized Tensile Fatigue Slope (18)
1	[0°/±45°/90°] Graphite	-4380	-5.52	
	Wet [0°/±45°/90°] Graphite	-4828	-6.42	
2	[0°/90°] Graphite	-7530	-6.62	
3	Woven Roving	-3030	-8.10	-16.5
4	Chopped Mat	-1930	-8.13	-9.6
5	[0°/90°] Glass	-5500	-8.32	-10.2
6	[0°/±45°] Graphite	-6520	-8.33	
	Wet [0°/±45°] Graphite	-6222	-8.74	
7	[0°/±45°/90°] Glass	-3930	-8.34	
8	[0°/±45°] Glass	-6219	-10.80	

TABLE 20

Cost-Effectiveness Comparisons

Materials	Density (lb/in^3)	UTS (lb/in^2)	Specific Strength $\frac{UTS}{\gamma} \times 10^6$	1978 Cost $/lb	Cost/ Specific Strength
Steels					
Low Carbon Structural Quenched & Tempered	.284	36,000	.127	.32	2.52
High Strength, Low Alloy, HY-100	.284	50,000	.176	.58	3.30
High Carbon	.284	60,000	.211	.36	1.71
Aluminum Alloys					
2024 T4	.100	42,000	.42	1.39	3.31
6061 T6	.098	35,000	.357	1.22	3.42
T300/5208*	.058	90,000	1.55	65.00**	41.93
Scotchply 1003*	.074	60,600	.819	3.16**	3.86
Woven Rovings	.065	35,000	.538	.60	1.11
Chopped Strand Mat	.070	19,430	.278	.55	1.98

* [0°/90°] Configuration

** estimate

AD-A072 690 NAVAL POSTGRADUATE SCHOOL MONTEREY CA F/G 11/4
COMPRESSIVE FATIGUE IN GLASS AND GRAPHITE REINFORCED COMPOSITES--ETC(U)
JUN 78 J D CONNERS

UNCLASSIFIED NL

2 OF 2
AD
A072690

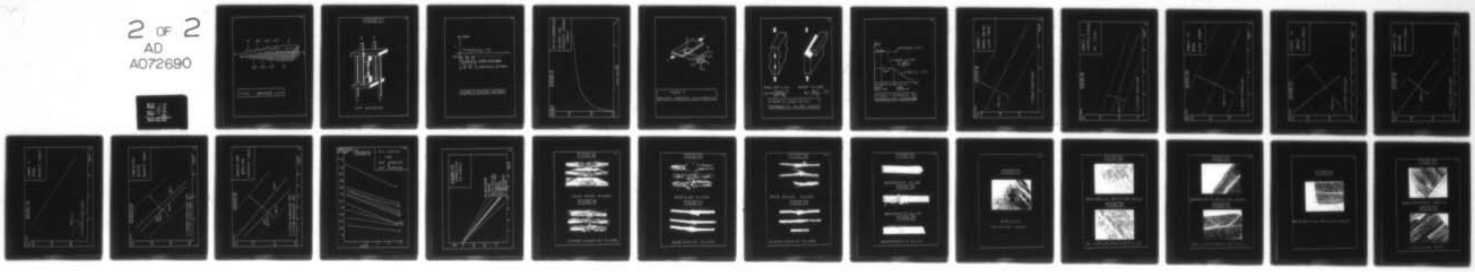

END
DATE
FILMED
9-79
DDC

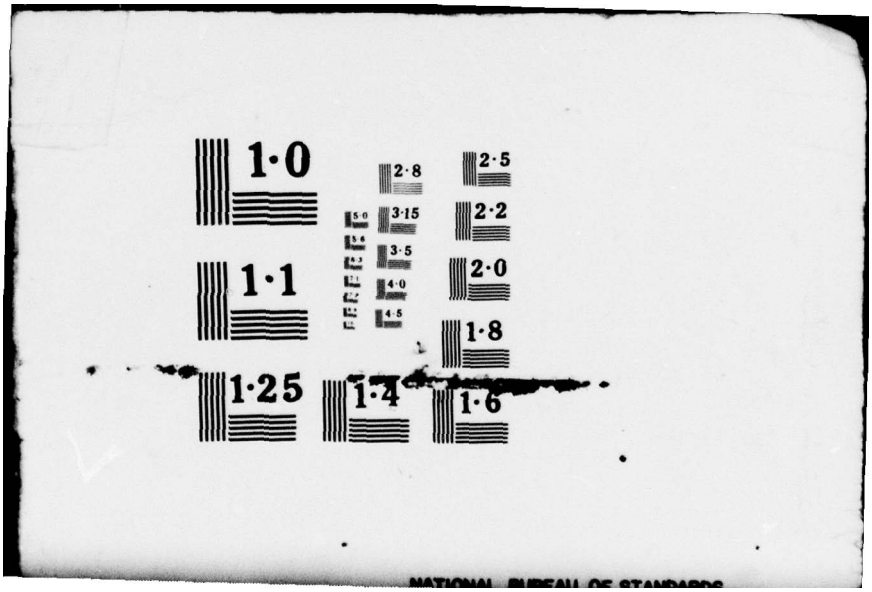
1·0
1·1
1·25
1·4
1·6
2·8
3·15
3·5
4·0
4·5
5·0
2·5
2·2
2·0
1·8

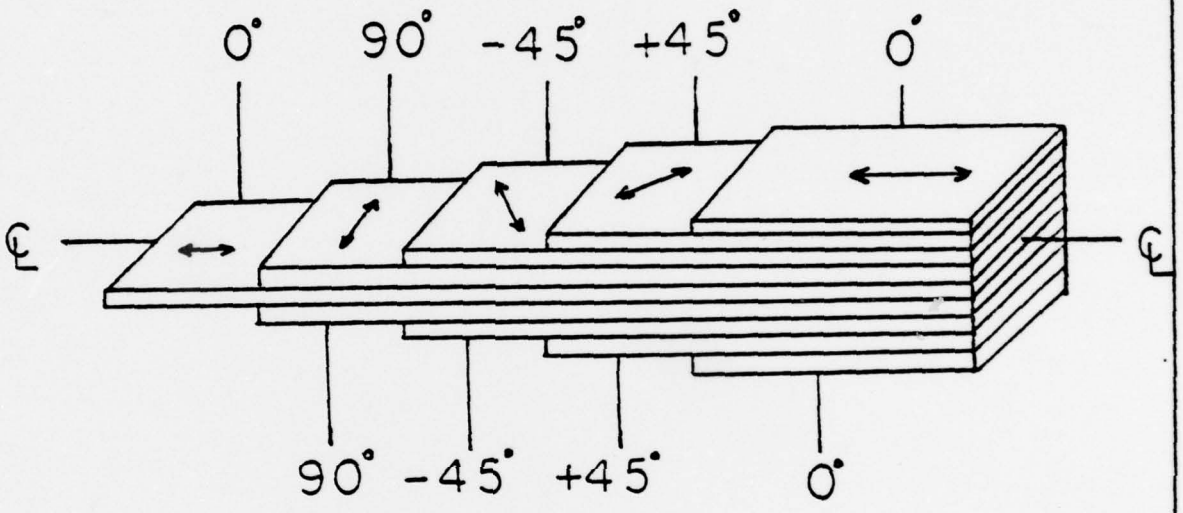

FIGURE 1 : [0/±45/90] LAYUP

FIGURE 2

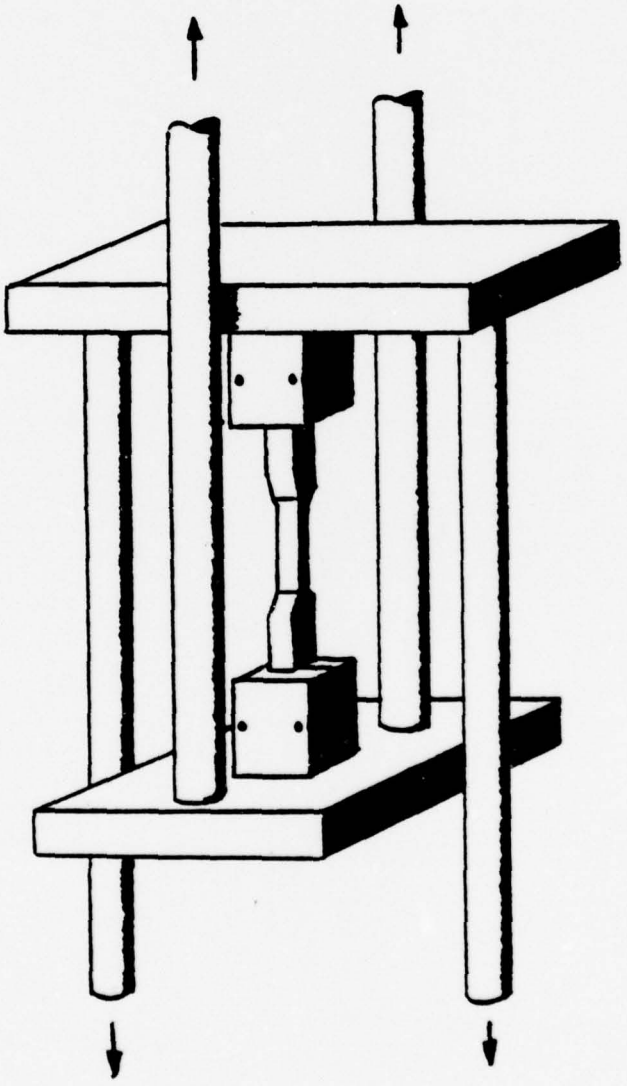

GRIP MECHANISM

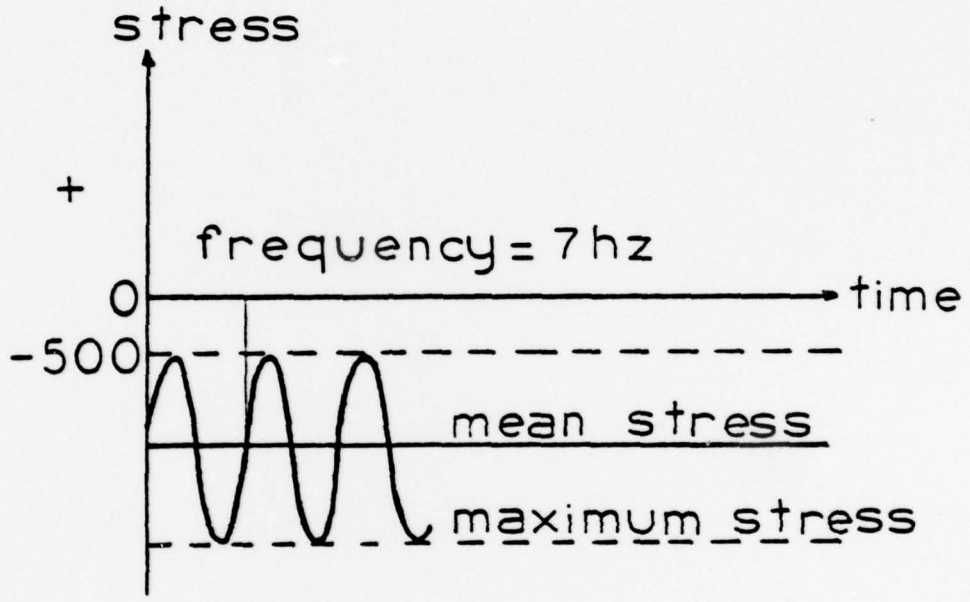

FIGURE 3: LOADING HISTORY

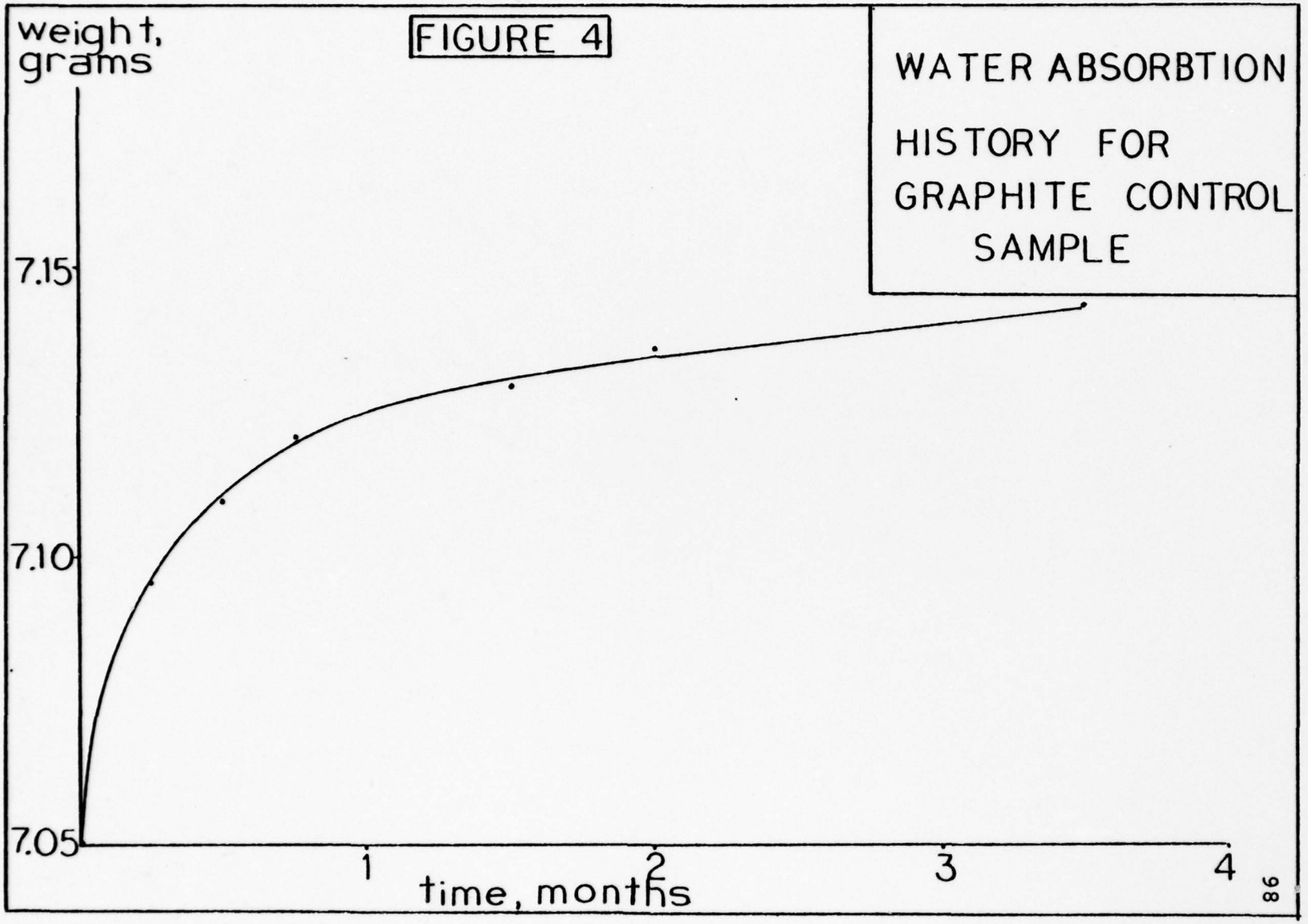
FIGURE 4
WATER ABSORBTION
HISTORY FOR
GRAPHITE CONTROL
SAMPLE
weight,
grams
7.15
7.10
7.05
1
2
3
4
time, months
86

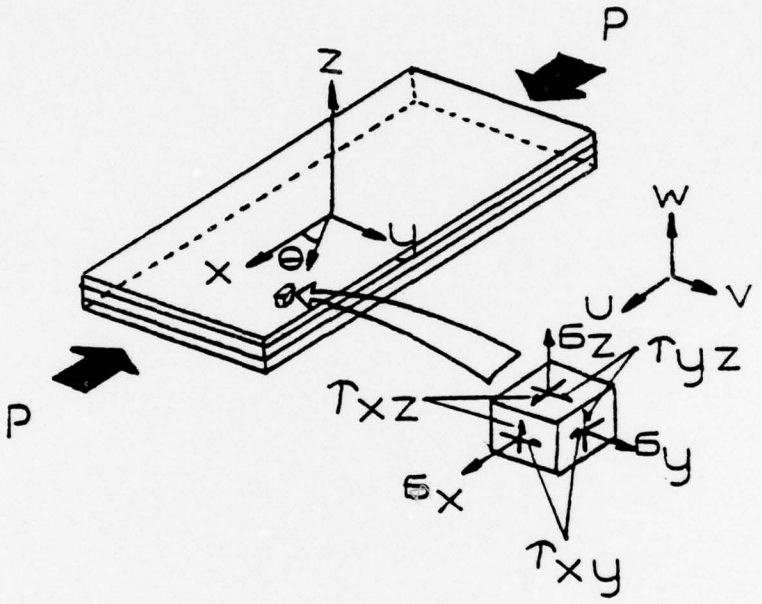

FIGURE 5

LAMINATE GEOMETRY AND STRESSES

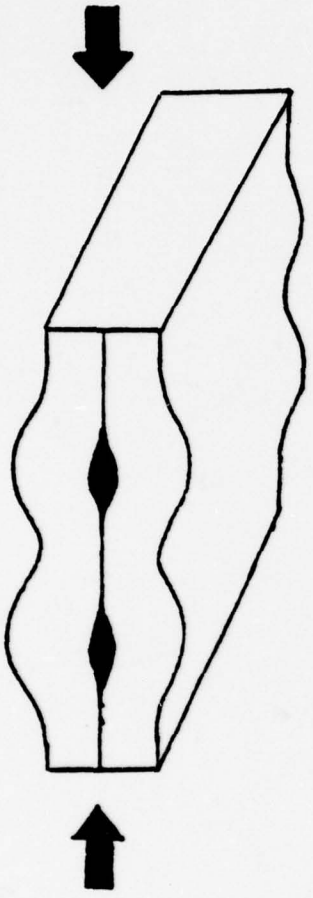

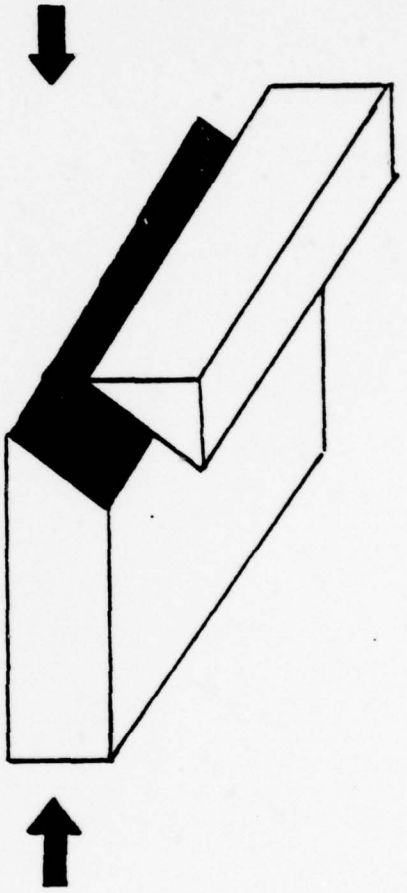

PANEL BUCKLING

$$\sigma_c = 2V_f\left[\frac{V_f E_f E_m}{3(1-V_f)}\right]^{\frac{1}{2}}$$

SHEAR FAILURE

$$\sigma_c = \frac{G_m}{(1-V_f)} \quad [4]$$

FIGURE 6: LONGITUDINAL COMPRESSIVE FAILURE MODES

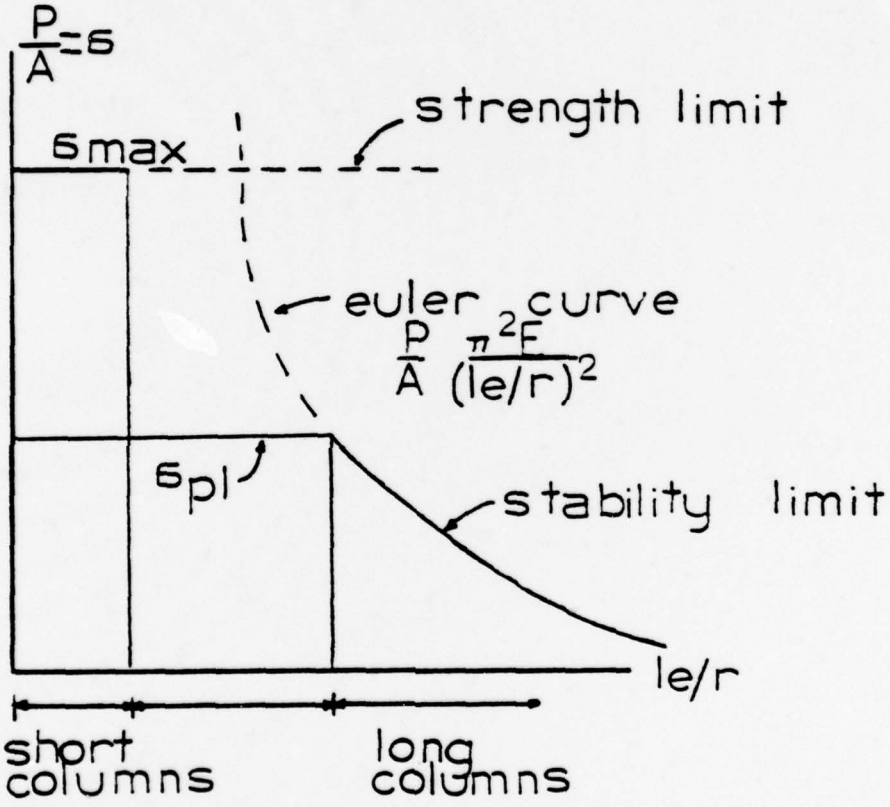

FIGURE 7 : STRESSES IN COMPRESSION MEMBERS[6]

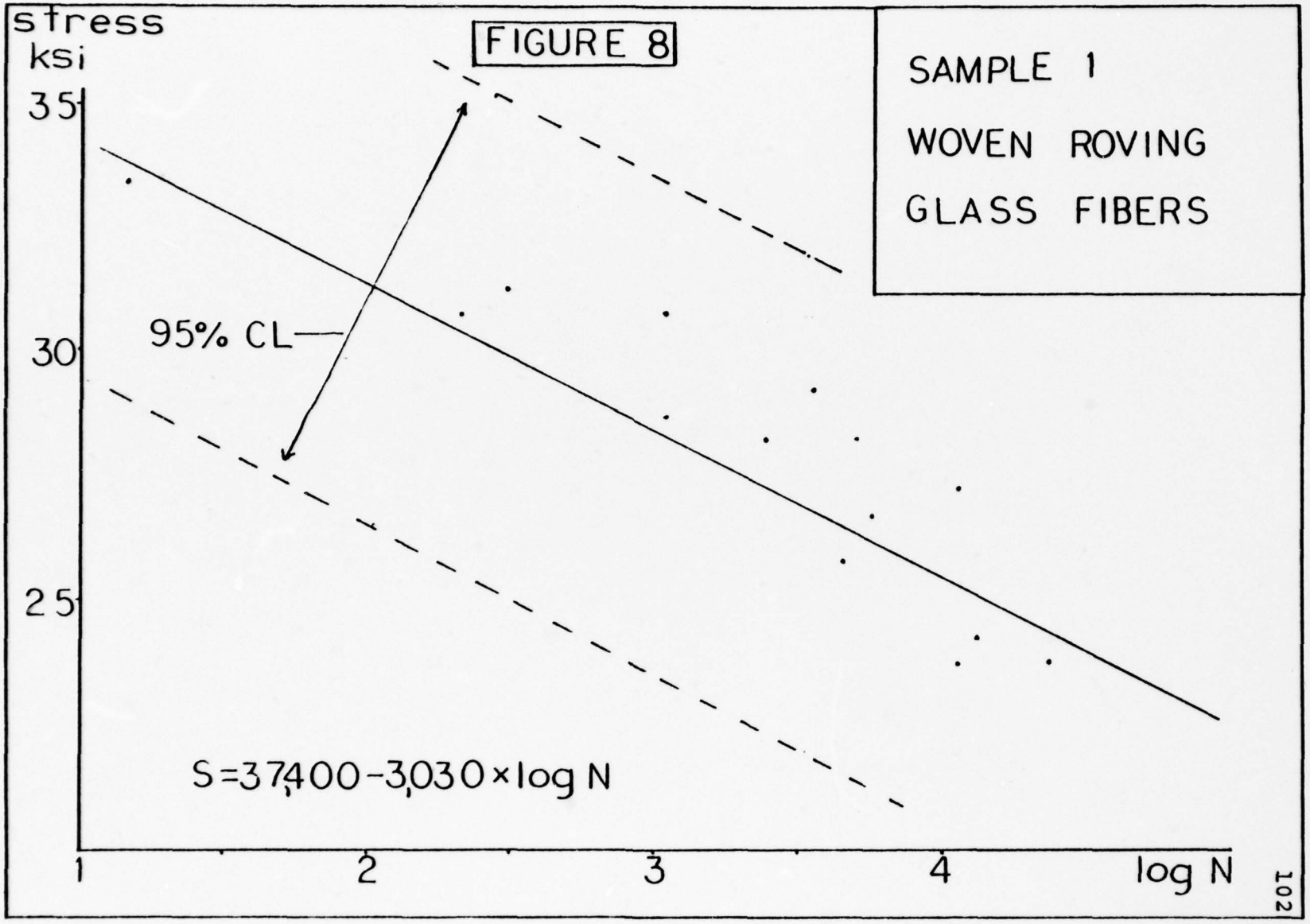
stress
ksi
35
30
25
95% CL
S=37,400-3,030×log N
1
2
3
4
log N
SAMPLE 1
WOVEN ROVING
GLASS FIBERS
102

FIGURE 8

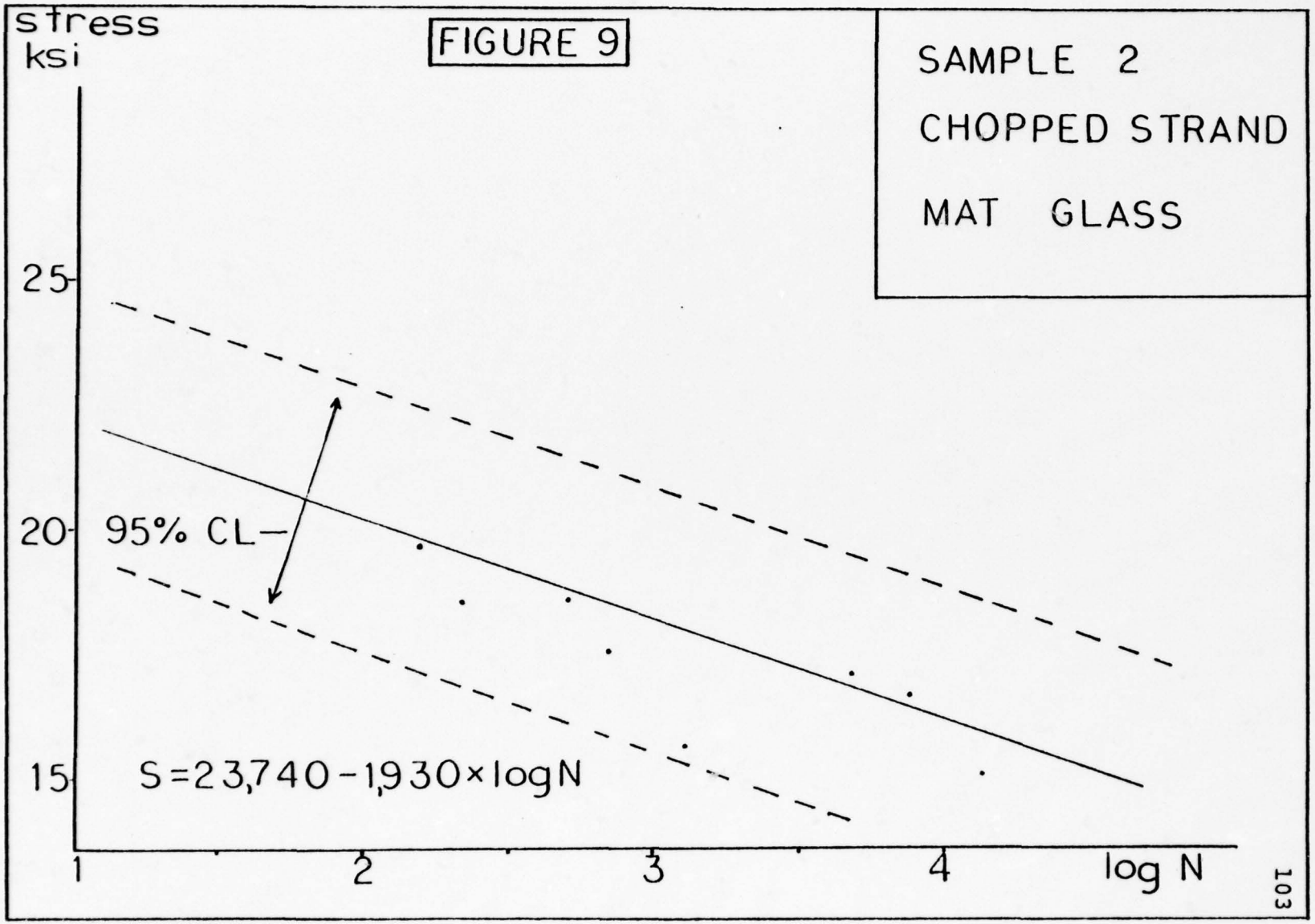
stress
ksi
FIGURE 9
SAMPLE 2
CHOPPED STRAND
MAT GLASS
25
20
15
95% CL
S=23,740-1,930×logN
1
2
3
4
log N
103

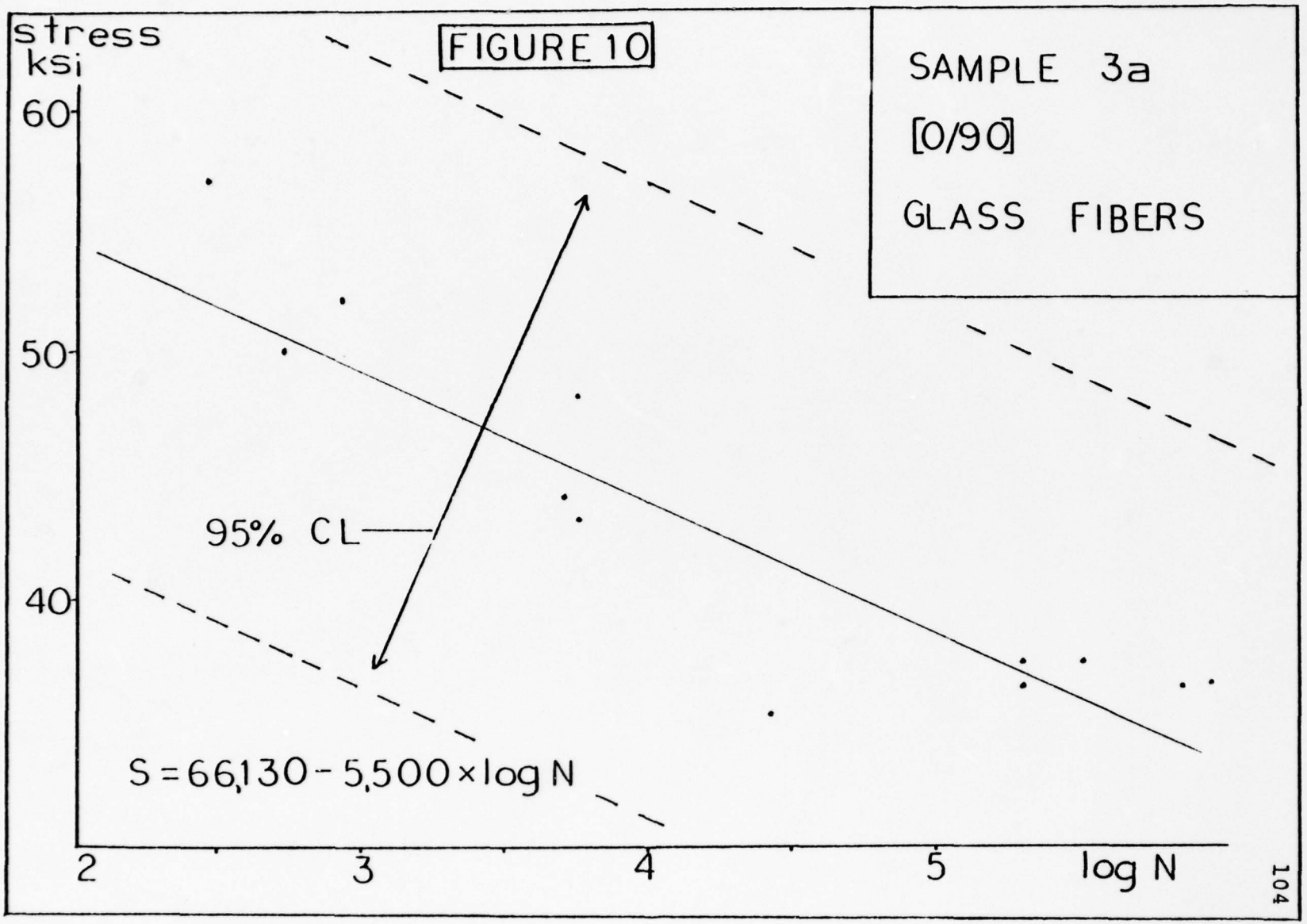
stress
ksi
FIGURE 10
SAMPLE 3a
[0/90]
GLASS FIBERS
60
50
40
95% CL
S = 66,130 - 5,500 × log N
2
3
4
5
log N
104

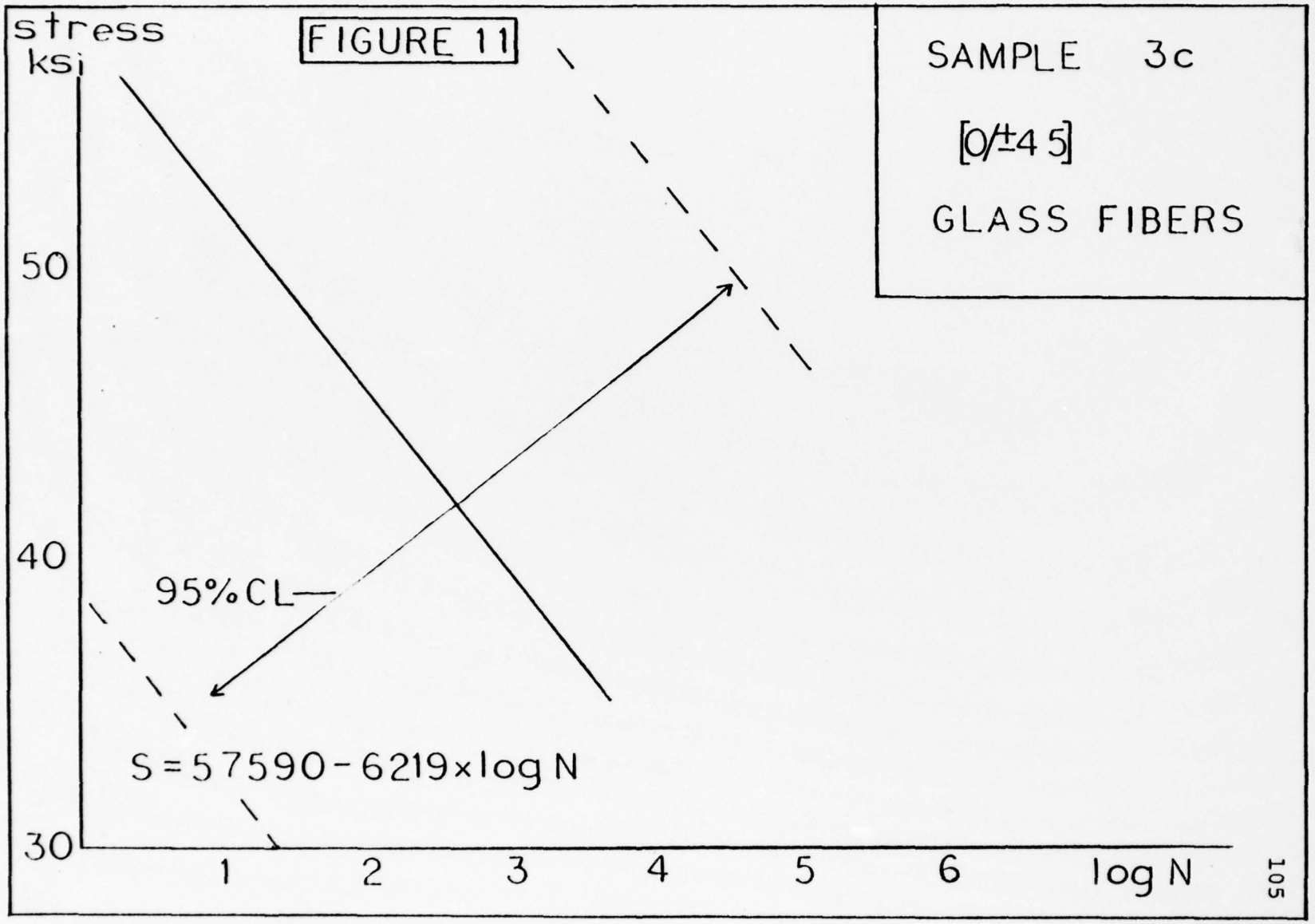
FIGURE 11
SAMPLE 3c
[0/±45]
GLASS FIBERS
stress
ksi
50
40
30
95% CL
S = 57590 - 6219 x log N
1
2
3
4
5
6
log N
105

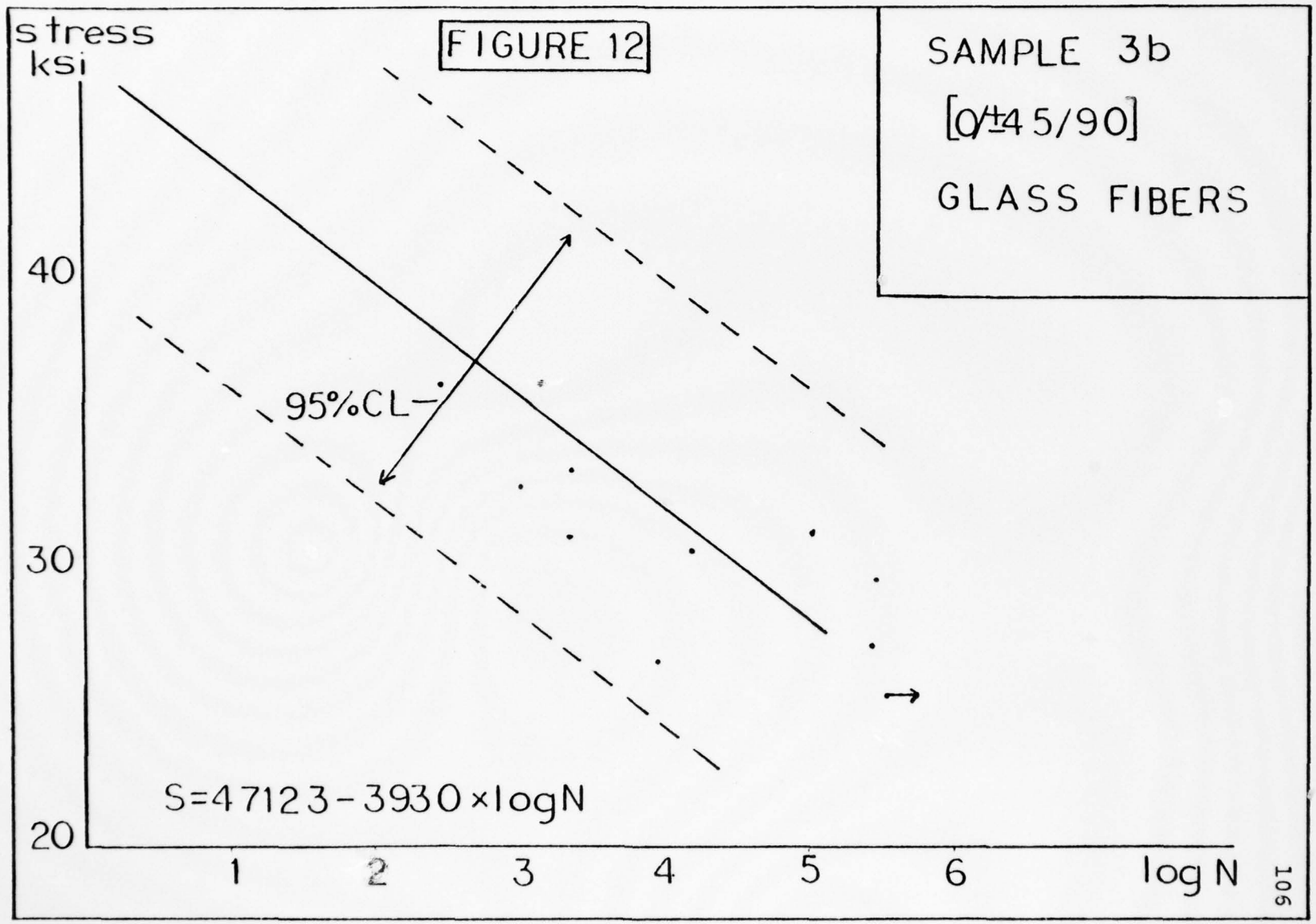
FIGURE 12
SAMPLE 3b
[0/±45/90]
GLASS FIBERS
stress
ksi
40
30
20
95%CL
S=47123-3930×logN
1
2
3
4
5
6
log N
106

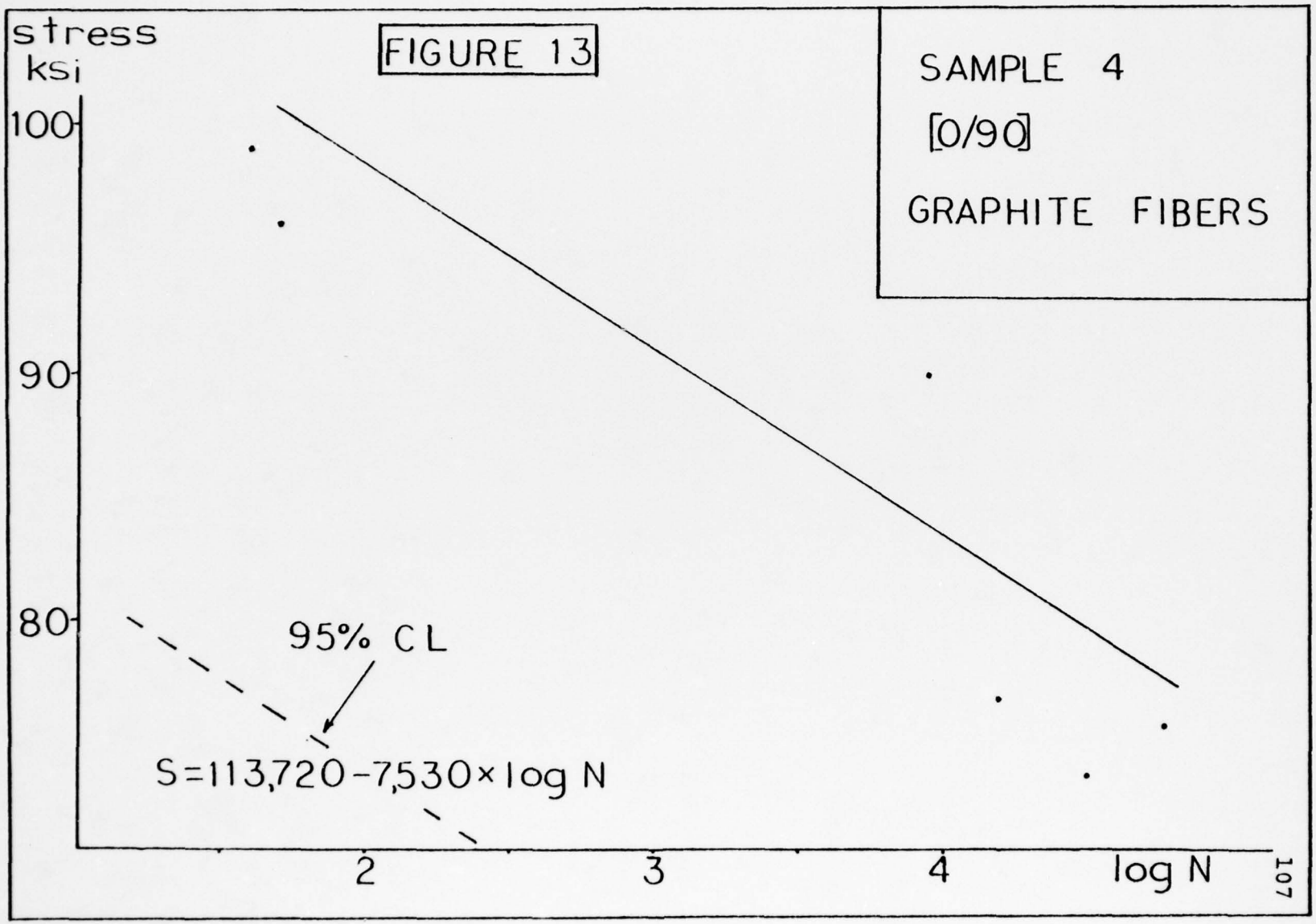
stress
ksi
FIGURE 13
SAMPLE 4
[0/90]
GRAPHITE FIBERS
100
90
80
95% CL
S=113,720-7,530×log N
2
3
4
log N
10^7

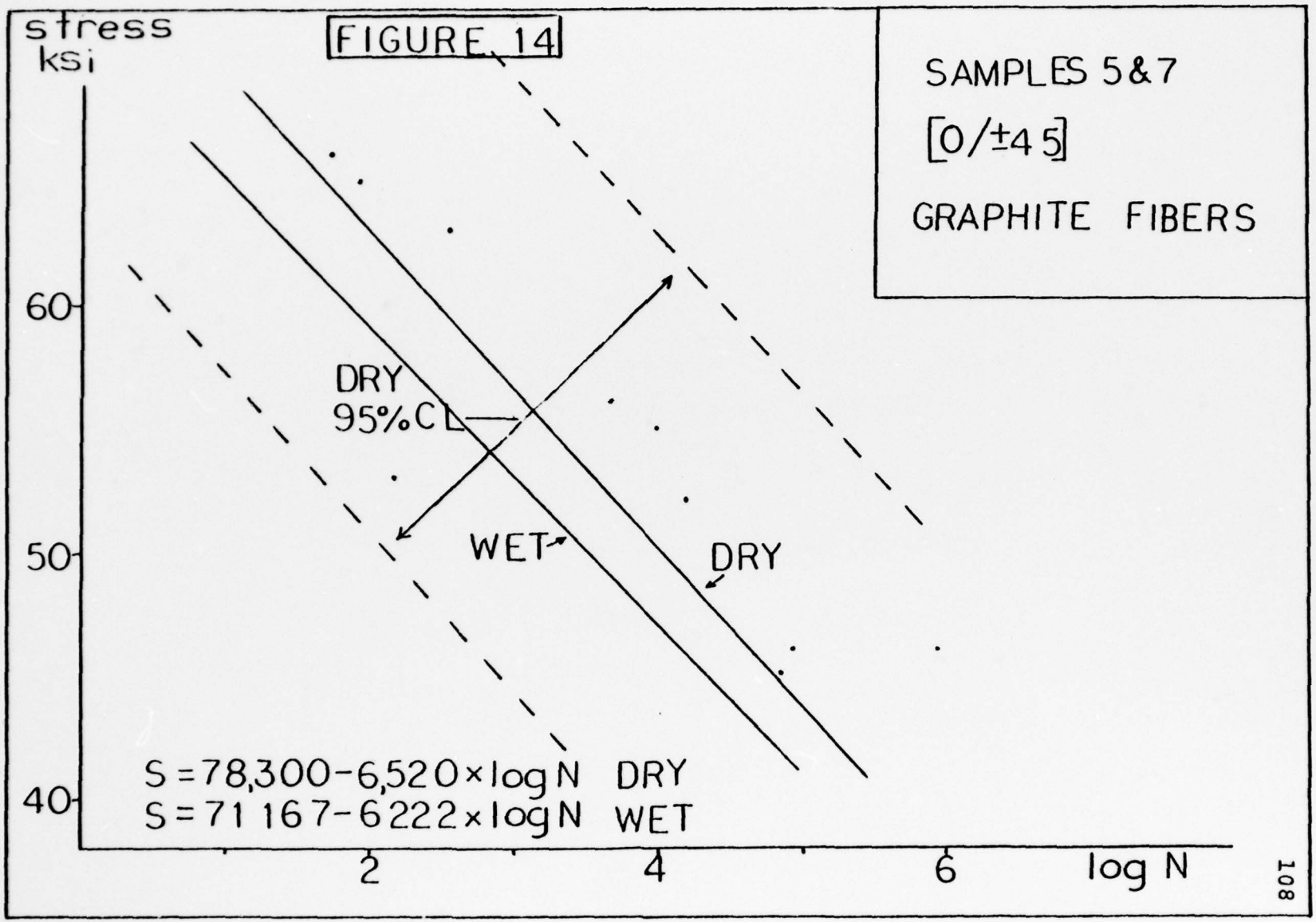
stress
ksi
FIGURE 14
SAMPLES 5&7
[0/±45]
GRAPHITE FIBERS
60
50
40
DRY
95%CL
WET
DRY
S = 78,300 - 6,520 × log N DRY
S = 71 167 - 6222 × log N WET
2
4
6
log N
108

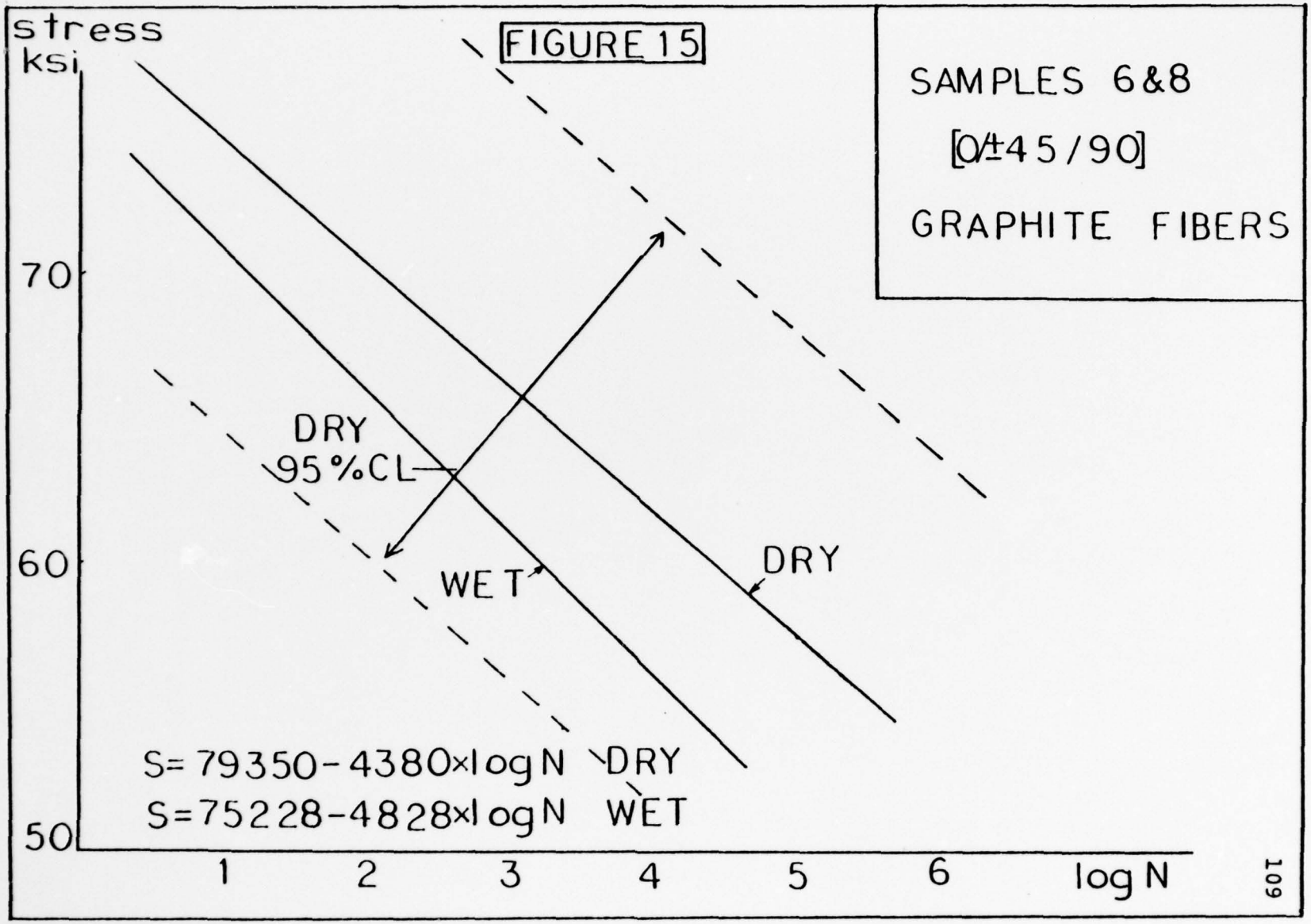
stress
ksi
FIGURE 15
SAMPLES 6&8
[0/±45/90]
GRAPHITE FIBERS
70
60
50
DRY
95%CL
WET
DRY
S= 79350-4380×log N DRY
S=75228-4828×log N WET
1
2
3
4
5
6
log N
109

FIGURE 16

S-N CURVES FOR DRY SAMPLES & WET SAMPLES

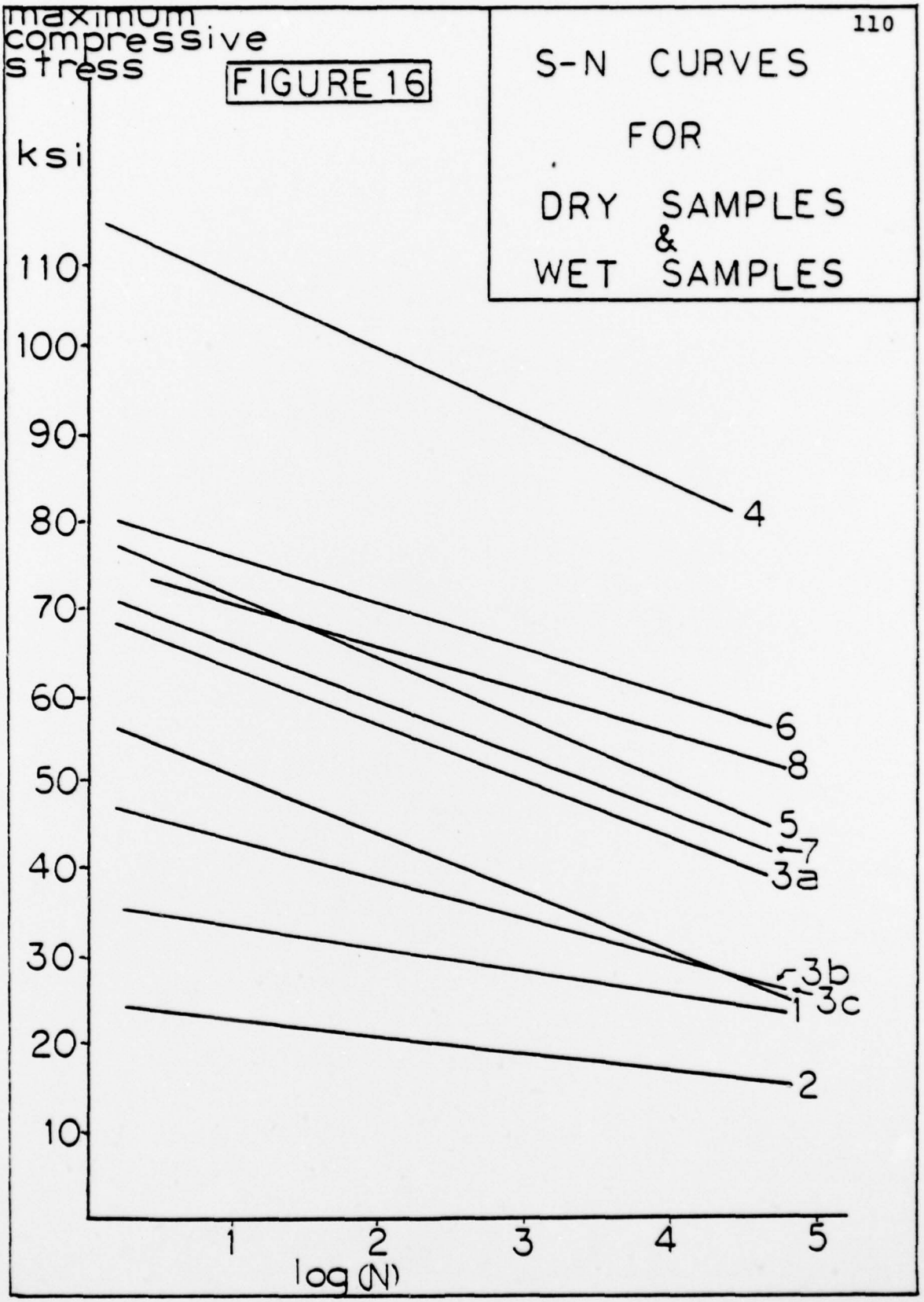

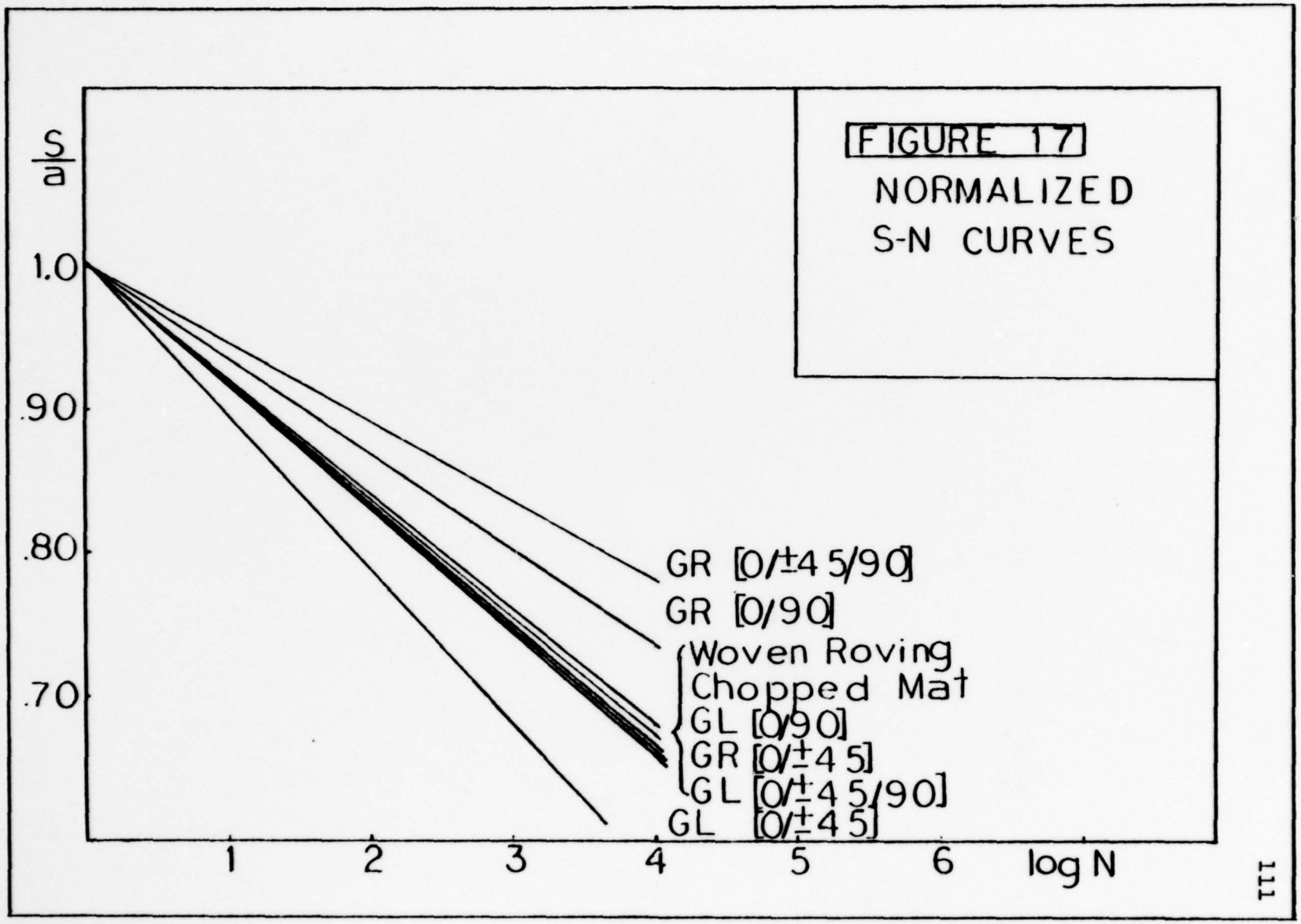
FIGURE 17
NORMALIZED
S-N CURVES
S/a
1.0
.90
.80
.70
GR [0/±45/90]
GR [0/90]
Woven Roving
Chopped Mat
GL [0/90]
GR [0/±45]
GL [0/±45/90]
GL [0/±45]
1
2
3
4
5
6
log N

FIGURE 18

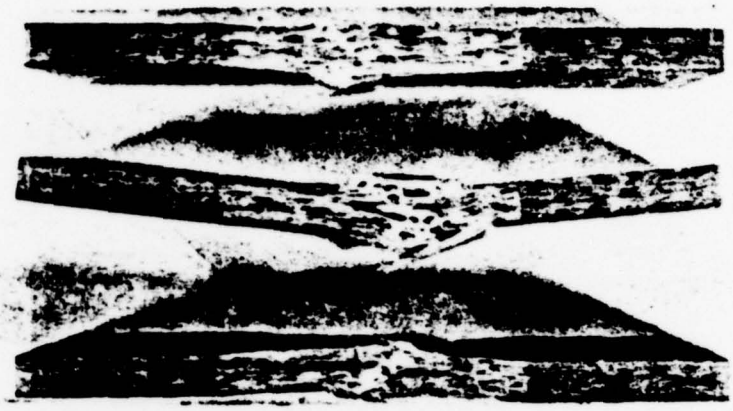

WOVEN ROVING FAILURES

FIGURE 19

CHOPPED STRAND MAT FAILURES

FIGURE 20

[0/90] GLASS FAILURES

FIGURE 21

[0/90] GRAPHITE FAILURES

FIGURE 22

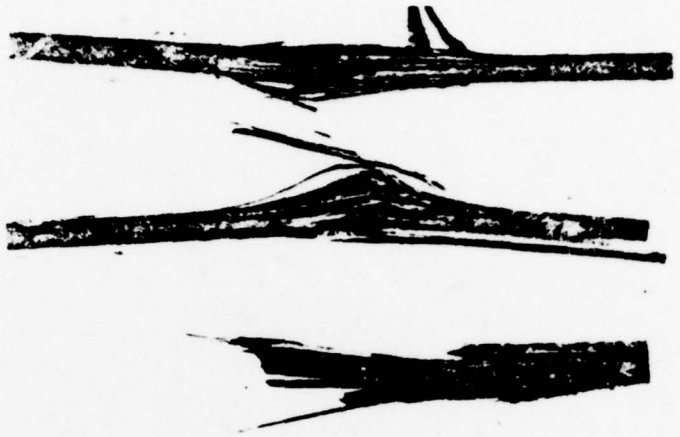

[0/±45] GRAPHITE FAILURES

FIGURE 23

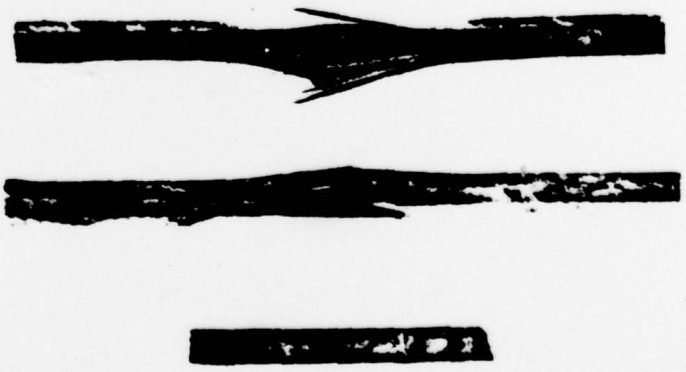

[0/±45/90] GRAPHITE FAILURES

FIGURE 24

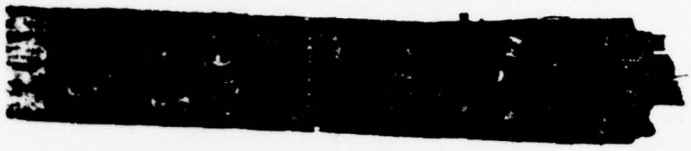

[0/90] GRAPHITE FAILURE

FIGURE 25

[0±45] GRAPHITE FAILURE

FIGURE 26

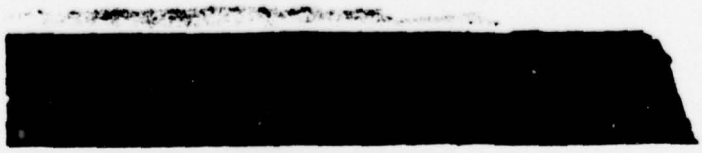

[0±45/90] GRAPHITE FAILURE

FIGURE 27

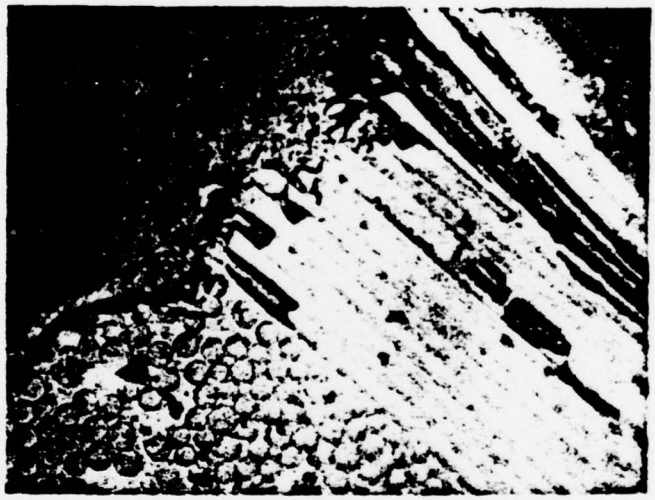

[0/90] GLASS

PRE-FAILURE DAMAGE

FIGURE 28

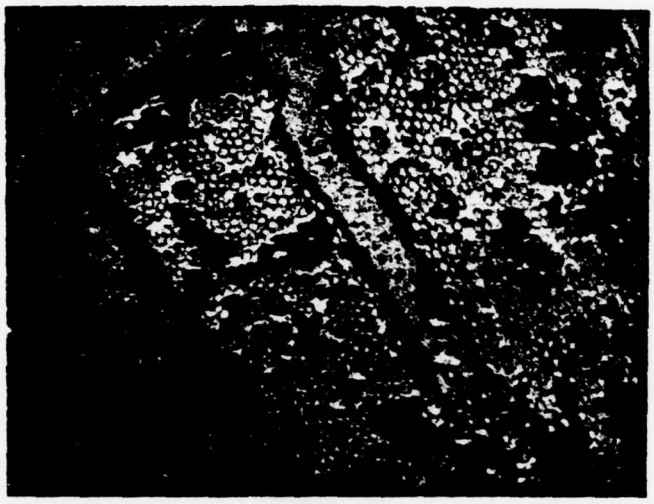

[0/±45/90] GLASS PRE-FAILURE DAMAGE

FIGURE 29

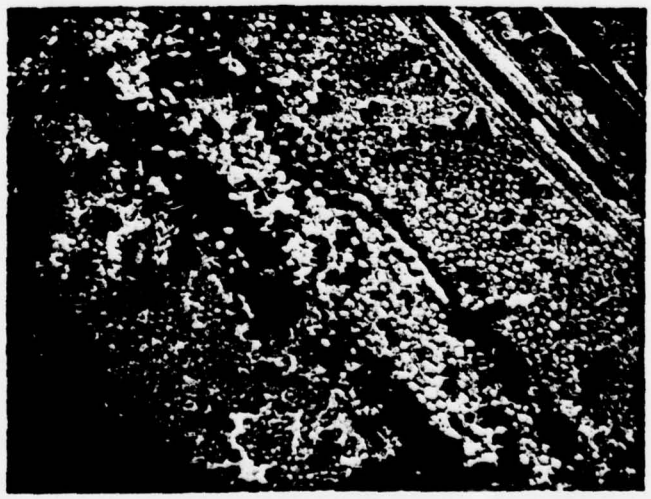

[0/±45/90] GLASS PRE-FAILURE DAMAGE

FIGURE 30

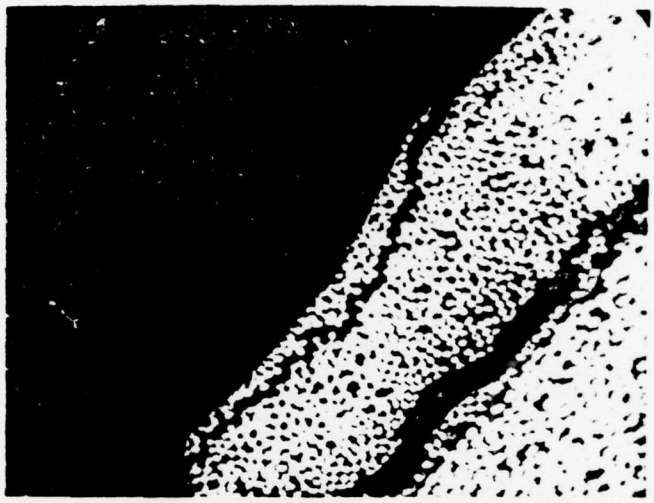

[0/±45] GRAPHITE PRE-FAILURE DAMAGE

FIGURE 31

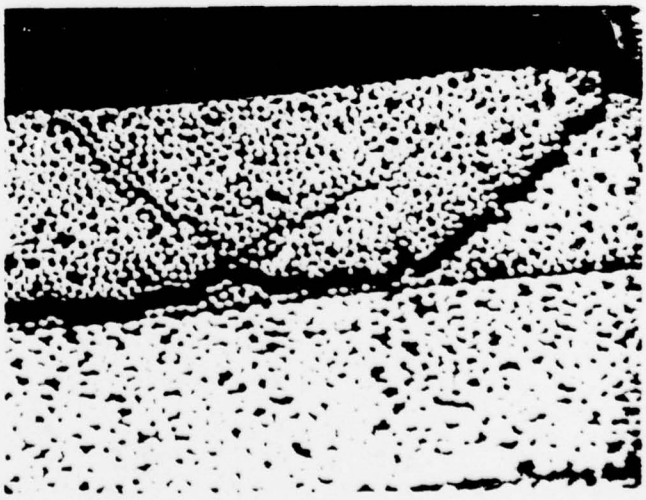

[0/±45] GRAPHITE PRE-FAILURE DAMAGE

FIGURE 32

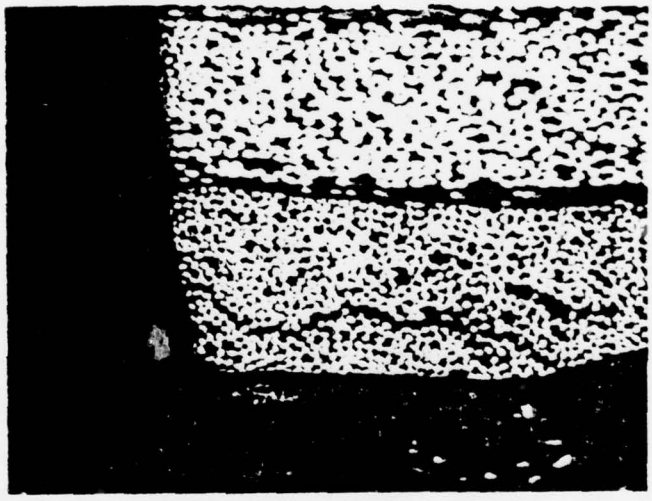

[0±4 5/9 0]GRAPHITE PRE-FAILURE DAMAGE

FIGURE 33

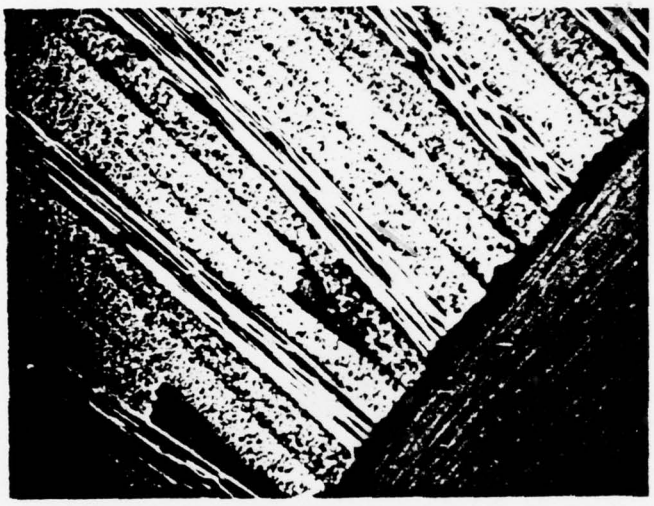

[0/±45/90] GRAPHITE DEFECTS

FIGURE 34

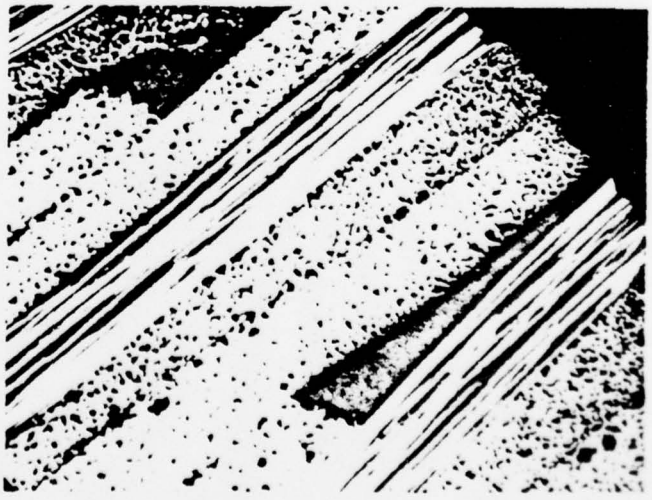

INTERLAMINAR DEFECT